Probabilistic Bearing Capacity Prediction of Square Footings on 3D Spatially Varying Cohesive Soils

Yajun Li, Ph.D.[1]; Gordon A. Fenton, Ph.D., M.ASCE[2]; Michael A. Hicks, Ph.D.[3]; and Nengxiong Xu, Ph.D.[4]

Abstract: The bearing capacity of square and/or rectangular footings in geotechnical foundation designs traditionally is determined based on experimental observations and/or deterministic analysis assuming uniform soil profiles. However, soils are spatially varying, and this spatial variability can significantly affect the bearing capacity of the foundation soils. Probability-based design methods can address this problem explicitly. However, a full three-dimensional (3D) probabilistic simulation, such as that involving the random finite-element method, generally is prohibitive, because it involves numerous Monte Carlo runs of a complicated nonlinear elastoplastic algorithm. This paper developed and validated an approximate analytical method based on local averaging theory and geometric averages of soil properties directly under the footing. It was found that the theoretical prediction of the first two moments of a square footing bearing capacity agrees very well with crude Monte Carlo simulation. The analytical prediction of the probability of a design failure was validated through simulation and can be used directly in reliability-based designs against bearing failure. **DOI: 10.1061/(ASCE)GT.1943-5606.0002538.**

Author keywords: Bearing capacity; Probability of failure; Shallow foundation; Spatial variability; Square footing.

Introduction

Geotechnical engineers routinely use the bearing capacity equation (Terzaghi 1943) to estimate the limit load that a foundation soil can sustain just before classical shear failure. For weightless soils (conservative), the bearing capacity of surface footings has the following form:

$$q_f = s_c \times c_u \times N_c \tag{1}$$

where q_f = ultimate bearing stress; c_u = undrained shear strength of soil; N_c = bearing capacity factor; and s_c = shape factor.

An exact solution for the bearing capacity factor of a footing on a purely cohesive soil is $N_c = 2 + \pi \approx 5.14$ (Prandtl 1920, 1921). For a strip footing, $s_c = 1.0$, whereas the following empirical expression for s_c commonly is used to evaluate the bearing capacity of footings with a finite length (Meyerhof 1951; Skempton 1951; Salgado et al. 2004):

$$s_c = 1 + 0.2(B/L) \tag{2}$$

where B = footing width; and L = footing length. For a square footing, $s_c = 1.20$. This paper focuses on square footings founded on a purely cohesive weightless soil.

The aforementioned procedure for calculating the bearing capacity of a square footing is based on the assumption that the soil on which the footing sits is uniform and characterized by a single soil property value. However, it is well known that soil properties are spatially variable and that this spatial variability (i.e., characterized by a so-called scale of fluctuation) influences soil behavior and the interaction between soils and structures (e.g., Nobahar 2003; Stuedlein et al. 2012; Li et al. 2014, 2015a, 2016a; Al-Bittar et al. 2018). Therefore, the statistics (e.g., mean and variance) of q_f change as a function of the variability in c_u. This raises the question of the reliability of q_f, and this reliability issue can be resolved quantitatively by considering explicitly the spatial variability involved.

In view of the nature of spatial variability, no plane strain solution [i.e., for a two-dimensional (2D) strip footing] exists that can be corrected simply for use in three-dimensions (e.g., a square footing). Despite soil spatial variability being naturally three-dimensional (3D) and the implication this has for footing bearing capacity, full three-dimensional probabilistic (random field) analyses of bearing capacity for the footing stability problem are surprisingly scarce. Recently, there have been a few first attempts toward the real three dimensional problem, either by trying to link with plane strain solutions or by using directly a full 3D analysis method. For example, Al-Bittar (2012) carried out a probabilistic analysis of a shallow foundation resting on a 3D random soil using a metamodel based on sparse polynomial chaos expansion combined with global sensitivity analysis (Al-Bittar and Soubra 2014a). Simoes et al. (2014) examined how a plane strain solution assuming no variation of soil properties in the third dimension can be related to the real strip footing resting on soils that vary in all three directions. In that case, no shape factor was needed, because they still considered the strip footing problem (i.e., the shapes were the same). Kawa et al. (2016) reported bearing capacity analyses of square footings using an overly simplified one-dimensional (1D) representation of soil property variability in the vertical direction. Kawa and Puła (2019) investigated a similar square footing founded on soils that varied spatially in three dimensions using a direct three-dimensional finite-difference analysis, without addressing the computational

[1]Lecturer, School of Engineering and Technology, China Univ. of Geosciences, Beijing 100083, China (corresponding author). ORCID: https://orcid.org/0000-0002-5863-5821. Email: y.j.li@cugb.edu.cn

[2]Professor, Dept. of Engineering Mathematics, Dalhousie Univ., Halifax, NS, Canada B3J 1B6.

[3]Professor, Dept. of Geoscience and Engineering, Delft Univ. of Technology, 2628 CN Delft, Netherlands.

[4]Professor, School of Engineering and Technology, China Univ. of Geosciences, Beijing 100083, China.

Note. This manuscript was submitted on January 11, 2020; approved on February 23, 2021; published online on April 8, 2021. Discussion period open until September 8, 2021; separate discussions must be submitted for individual papers. This paper is part of the ***Journal of Geotechnical and Geoenvironmental Engineering***, © ASCE, ISSN 1090-0241.

efficiency issue. Chwała (2019) proposed a kinematics-based approach to estimating the random bearing capacity of square and rectangular foundations, based on previous 2D studies (Puła and Chwała 2015, 2018). Li et al. (2020) proposed a way to cope with this 3D complexity by modifying the shape factor defined in Eq. (1), based on 3D analyses of both strip and square footings for various site variability conditions, to ensure a consistent reliability of the bearing capacity evaluation. However, this treatment sometimes could be misleading, due to a modification of the shape factor implying a change of the foundation shape, whereas it actually only involves the spatial variability of c_u in Eq. (1). Apart from this confusion, the analyses needed to arrive at a reasonable value of s_c that can be used directly in Eq. (1) are computationally costly due to the involvement of complicated 3D nonlinear elastoplastic analyses. Some 3D investigations of deep foundations are available (Vahdatirad et al. 2013; Li et al. 2017a, b; El Haj et al. 2019; El Haj and Soubra 2020), although the present investigation primarily focused on 3D shallow foundations, and so those investigations were not pursued further here.

With reference to Eq. (1), there are two alternative ways to find bearing capacity solutions of square footings resting on 3D soils: one is to derive a relationship between the 2D plane strain bearing capacity solution, which assumes an infinite scale of fluctuation in the out-of-plane direction, and the full 3D solution [although this is a costly exercise, because no simple relationship exists (Li et al. 2020)]; the other is to use an analogy of the 2D bearing capacity equation for the square footing, without resorting to s_c, that is

$$q_f = c_u \times N_c' \tag{3}$$

where N_c' = deterministic bearing capacity factor for square footing (which may be defined in this case as $N_c' \approx 1.2 \times 5.14$). This approach avoids the problem of modifying the shape factor, and, in the case of spatially varying c_u, c_u can be replaced by $\bar{c}_u$, which is an effective value of c_u that accounts for the spatial variability of the soil in the failure zone.

Therefore, instead of trying to provide a link between the statistics of the 2D solution and those of the real 3D square footing solution, this paper solved the problem by using the 3D counterpart of Eq. (1), that is, Eq. (3) with c_u replaced by $\bar{c}_u$. However, it is quite challenging to find $\bar{c}_u$ without resorting to costly numerical analyses using methods such as the finite-element method or finite-difference method (Ching et al. 2014, 2015, 2016a). Fenton and Griffiths (2003) proposed using geometric averages over some domain below the footing to represent $\bar{c}_u$, based on rigorous local averaging derivations and verification against random finite-element analysis (FEA) results of a strip footing problem in two dimensions. The present paper extends the theoretical work of Fenton and Griffiths (2003) to three dimensions and examines the variability of q_f for square footings supported by 3D spatially varying clay soils. The importance of the theoretical work of Fenton and Griffiths (2003) is obvious; properly extended to three dimensions and validated, it can be used to derive analytically the first two moments of q_f for a square footing, thereby avoiding the enormous computational resources that otherwise would be required. Although the extension to three dimensions is relatively straightforward, there are distinct features and open questions for 3D problems [compared with 2D problems, e.g., Ching et al. (2016b)] requiring further systematic investigation. For example, due to the failure path in three dimensions being a surface, the degree of spatial averaging or magnitude of variance reduction is different by a significant amount. Therefore, the calculated probability of failure also differs significantly in magnitude. In addition, there is the follow-up question about whether a simple extension of the 2D averaging domain size to three dimensions is applicable, due to the different degree of spatial averaging. If it is not applicable in three dimensions, what averaging domain size should be used in three dimensions? How does it change when the spatial variability characteristics (e.g., coefficient of variation or correlation scale) change? Moreover, what are the bounds of the solution, and how do they help explain the solution behavior? How good are the mean and variance estimators? These are all open questions that need to be answered through a detailed investigation. Because most problems encountered in practice are 3D, it seems natural to turn to 3D studies, as opposed to the numerous 2D studies in the literature.

This paper starts by reviewing the random field model used to represent the soil spatial variability. The theoretical model then is introduced, followed by a verification through Monte Carlo (MC) simulation of the square footing problem in terms of both the two moments and the probability of a design failure of the square footing. In contrast to the previous 2D study (Fenton and Griffiths 2003), this paper presents a systematic investigation of the probability of failure and its confidence intervals (CIs) for various scenarios of spatial variability; i.e., it explores the conditions in which the theoretical predictions can be used confidently and conditions in which they can be used only as preliminary indicators of the foundation safety level. It is important to focus on the probability of failure, because a slight error in the estimate of the mean could result in a large error in the failure probability estimate, depending on the variance estimate.

Random Field Model

In practical geotechnical applications, random fields have been used extensively for representing the spatial variation of soil properties (Fenton and Griffiths 2008; Li et al. 2015b, 2016b; Luo and Bathurst 2017; Hicks and Li 2018). The generation of a random field of soil properties requires as input the following statistical parameters: the mean value (μ), the standard deviation (σ) or variance (σ^2), and the correlation length or scale of fluctuation (SOF) (θ) that characterizes generally the spatial fluctuation scale of the spatially varying soil property. The coefficient of variation (COV) ($v_c = \sigma/\mu$) alternatively can be provided instead of the standard deviation, and the scale of fluctuation is associated with some form of correlation function to describe the correlation coefficient between any pair of points in space (Vanmarcke 1977, 1978, 1983).

Of the various methods of generating/discretizing random fields (Matthies et al. 1997), the spatial averaging method (Vanmarcke and Grigoriu 1983) or local average subdivision (LAS) method (Fenton and Vanmarcke 1990) was used in this paper. According to Der Kiureghian and Ke (1987), stochastic finite-element analysis using LAS as a random field discretization method can produce relatively accurate results of structural reliability even when using rather coarse meshes. Due to the consistency in modeling the variance for different element sizes in the mesh, LAS combined with a relatively coarse mesh yields quite good results, as is shown in the following sections.

In this study, the soil undrained shear strength (c_u) was assumed to be characterized by a stationary, lognormally distributed random field, with mean μ_{c_u}, standard deviation σ_{c_u}, and an exponential correlation structure parameterized with the scale of fluctuation θ_{c_u}. A lognormally distributed random field is generated by transforming a normally distributed random field (i.e., the underlying field) $S_{\ln c_u}(\boldsymbol{x})$ with zero mean, unit variance, and scale of fluctuation $\theta_{\ln c_u}$ through

$$c_u(\boldsymbol{x}) = \exp(\mu_{\ln c_u} + \sigma_{\ln c_u} S_{\ln c_u}(\boldsymbol{x})) \tag{4}$$

where $\boldsymbol{x}$ = spatial coordinates; and $\mu_{\ln c_u}$ and $\sigma_{\ln c_u}$ = mean and standard deviation of the underlying normal random field, respectively. The following relationships are used to transform from c_u space to $\ln c_u$ space:

$$\sigma^2_{\ln c_u} = \ln\left(1 + \frac{\sigma^2_{c_u}}{\mu^2_{c_u}}\right) \tag{5a}$$

$$\mu_{\ln c_u} = \ln \mu_{c_u} - (1/2)\sigma^2_{\ln c_u} \tag{5b}$$

These transformation equations hold for any lognormally distributed variable. The section "Monte Carlo Simulation versus Theoretical Predictions" shows that q_f follows a lognormal distribution, so Eqs. (5*a*) and (5*b*) are equally applicable when using the subscripts q_f and $\ln q_f$.

The correlation structure is characterized here by a correlation function of a simple exponential form parameterized by the scales of fluctuation $\theta^v_{\ln c_u}$ and $\theta^h_{\ln c_u}$ in the vertical and horizontal directions, respectively

$$\rho_{\ln c_u}(\tau_1, \tau_2, \tau_3) = \exp\left(-\frac{2|\tau_3|}{\theta^v_{\ln c_u}} - \sqrt{\left(\frac{2\tau_1}{\theta^h_{\ln c_u}}\right)^2 + \left(\frac{2\tau_2}{\theta^h_{\ln c_u}}\right)^2}\right) \tag{6}$$

where $\boldsymbol{\tau} = \{\tau_1, \tau_2, \tau_3\}^T = \boldsymbol{x} - \boldsymbol{x}'$ = separation distance vector between two spatial points $\boldsymbol{x}$ and $\boldsymbol{x}'$. Eq. (6) has a partially separable form in τ_3 (vertically) due to geological layer deposition. This correlation function governs the underlying Gaussian random fields, as indicated by the subscript $\ln c_u$ of ρ. Although this study conducted investigations based only on the isotropic correlation structure (i.e., $\theta^h_{\ln c_u} = \theta^v_{\ln c_u} = \theta_{\ln c_u}$) because the objective was to focus on the fundamental stochastic behavior of bearing capacity for the simplest case, the more general form of an anisotropic correlation function with two fluctuation scales was retained.

Based on the preceding random field model, it is possible to produce a series of random field realizations of spatially varying soil properties. For illustrative purposes, Figs. 1(a and b) are example realizations of spatially varying $\ln c_u$ fields characterized by relatively small or large SOFs, with strong and weak soils represented by darker and lighter regions, respectively.

Theoretical Model

The idea of using the statistics of a geometric average over some domain directly below the footing to predict the mean and variance of bearing capacity of spatially varying soils was proposed by Fenton and Griffiths (2003) for a plane strain strip footing. In view of the weakest link phenomenon in which soils seek out the weakest path possible in bearing stability problems, the geometric average is a good choice because it is low-value dominated. Very good predictions of the mean and variance of strip footing bearing capacity were obtained by Fenton and Griffiths (2003). This paper therefore extends their study to square footings on a three dimensional heterogeneous soil to validate the applicability in three dimensions. The emphasis here is on the 3D characteristics of the model and the theoretical bounds of the mean solution as a function of the scale of fluctuation, which is necessary to assess the error and confidence of the mean and probability of failure predictions for a variety of possible inputs in the section "Monte Carlo Simulation versus Theoretical Predictions." It is postulated that, for a square footing on a spatially uniform soil, Eq. (3) could be used by replacing c_u with some effective value $\bar{c}_u$, which in this case is the geometric average over some rectangular cuboid domain directly under the footing; that is

$$q_f = \bar{c}_u \times N'_c \tag{7}$$

This assumes that soils with spatially varying c_u have the same bearing capacity as soils that are spatially uniform but with an effective/equivalent $\bar{c}_u$. The geometric average $\bar{c}_u$ over some continuous soil domain D, of size $L_x \times L_y \times L_z$, is defined as

$$\bar{c}_u = \exp\left(\frac{1}{L_x L_y L_z}\int_0^{L_z}\int_0^{L_y}\int_0^{L_x} \ln c_u(\boldsymbol{x}) dx dy dz\right) \tag{8}$$

where $\boldsymbol{x} = (x, y, z)$ is a point in space.

When discretized into a series of nonoverlapping soil elements, such as in finite elements, $\bar{c}_u$ is given as

$$\begin{aligned}\bar{c}_u &= \left(\prod_{i=1}^{n} c_u(\boldsymbol{x_i})\right)^{1/n} = \exp\left(\frac{1}{n}\sum_{i=1}^{n} \ln c_u(\boldsymbol{x_i})\right) \\ &= \exp\left[\frac{1}{n}\sum_{i=1}^{n}(\mu_{\ln c_u} + \sigma_{\ln c_u} S_{\ln c_u}(\boldsymbol{x_i}))\right] \\ &= \exp(\mu_{\ln c_u} + \sigma_{\ln c_u} \bar{S}^a_{\ln c_u})\end{aligned} \tag{9}$$

where n = number of nonoverlapping rectangular cuboid elements to be averaged below the footing; $\boldsymbol{x_i}$ = ith element location in space; and

$$\bar{S}^a_{\ln c_u} = \frac{1}{n}\sum_{i=1}^{n} S_{\ln c_u}(\boldsymbol{x_i}) \tag{10}$$

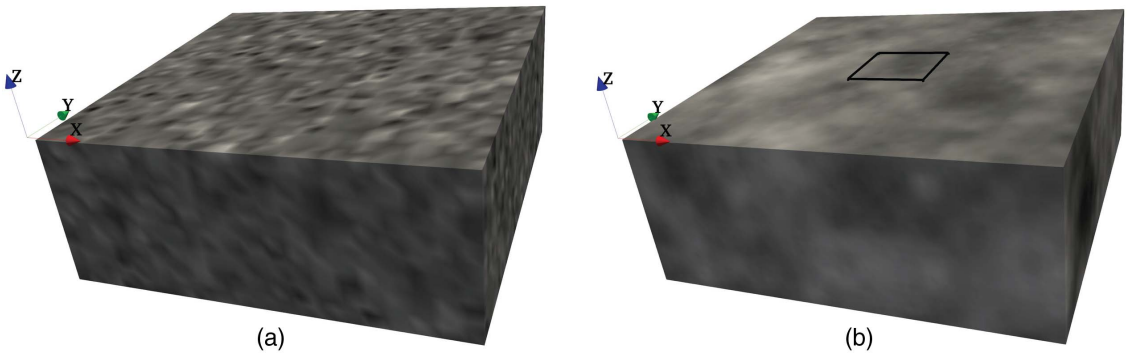

Fig. 1. Example spatial variability illustration of $\ln c_u$ with different scales of fluctuation and domain size $5 \times 5 \times 2$ m: (a) $\theta_{\ln c_u} = 0.1$ m; and (b) $\theta_{\ln c_u} = 2$ m.

J. Geotech. Geoenviron. Eng., 2021, 147(6): 04021035

is the arithmetic average of $S_{\ln c_u}(\boldsymbol{x})$ over domain D. Superscript a is used for $\bar{S}$ to distinguish it from $\bar{c}_u$, in which the overbar indicates a geometric average. The derivation in Eq. (9) makes use of Eq. (4).

Eq. (7) can be nondimensionalized by dividing by the mean of c_u, thus defining the stochastic bearing capacity factor M_c

$$M_c = \frac{q_f}{\mu_{c_u}} = \frac{\bar{c}_u N_c'}{\mu_{c_u}} \tag{11}$$

Because c_u is assumed to be log-normally distributed, $\bar{c}_u$ also is log-normally distributed acoording to Eq. (9), which in turn implies a log-normal distribution for q_f [Eq. (7), where N_c' is constant for cohesive soils] and M_c [Eq. (11)]. Thus, taking logarithms of Eq. (11) gives

$$\ln M_c = \ln q_f - \ln \mu_{c_u} = \ln \bar{c}_u + \ln N_c' - \ln \mu_{c_u} \tag{12}$$

Statistical Moments of $\ln M_c$

The problem now is to find the mean and variance of the normally distributed $\ln M_c$. The mean of $\ln M_c$ is

$$\mu_{\ln M_c} = \mu_{\ln \bar{c}_u} + \ln N_c' - \ln \mu_{c_u} \tag{13}$$

The terms $\ln N_c'$ and $\ln \mu_{c_u}$ are constants for any given μ_{c_u}; N_c' can be given simply as 1.2×5.14 or determined by a single deterministic finite-element analysis based on μ_{c_u} [Eq. (3)]. The term $\mu_{\ln \bar{c}_u}$ can be obtained by taking logarithms of Eq. (9) as follows:

$$\mu_{\ln \bar{c}_u} = E[\mu_{\ln c_u} + \sigma_{\ln c_u} \bar{S}^a_{\ln c_u}] = \mu_{\ln c_u} + \sigma_{\ln c_u} E[\bar{S}^a_{\ln c_u}] \tag{14}$$

where $E[\cdot]$ denotes the expectation operator.

According to Eq. (10) and local averaging theory (Vanmarcke 1983), the expectation of $\bar{S}^a_{\ln c_u}$ is zero, that is

$$E[\bar{S}^a_{\ln c_u}] = E[S_{\ln c_u}] = 0 \tag{15}$$

Therefore, $\mu_{\ln \bar{c}_u} = \mu_{\ln c_u}$, so Eq. (13) can be expressed as

$$\mu_{\ln M_c} = \mu_{\ln c_u} + \ln N_c' - \ln \mu_{c_u} \tag{16}$$

Combining Eqs. (5) and (16) gives

$$\mu_{\ln M_c} = \ln N_c' - 0.5 \ln\left(1 + \frac{\sigma^2_{c_u}}{\mu^2_{c_u}}\right) \tag{17}$$

In Eq. (12), the variance of $\ln M_c$ equals the variance of $\ln \bar{c}_u$, that is

$$\sigma^2_{\ln M_c} = \sigma^2_{\ln \bar{c}_u} \tag{18}$$

The variance of $\ln \bar{c}_u$ can be obtained by taking logarithms of Eq. (9) and using basic properties of variance operation, that is

$$\sigma^2_{\ln \bar{c}_u} = \sigma^2_{\ln c_u} \times \sigma^2_{\bar{S}^a_{\ln c_u}} \tag{19}$$

According to Eq. (10) and local averaging theory (Vanmarcke 1983), the variance of $\bar{S}^a_{\ln c_u}$ is given by $\sigma^2_{\bar{S}^a_{\ln c_u}} = \gamma(D) \times \sigma^2_{S_{\ln c_u}}$, where $\sigma^2_{S_{\ln c_u}} = 1.0$ and $\gamma(D)$ is the variance reduction function that quantifies the ratio between the variance of arithmetic local averages over domain D and the variance of the point process.

Substitution of Eq. (19) into Eq. (18) leads to the following expression for the variance of $\ln M_c$:

$$\sigma^2_{\ln M_c} = \gamma(D)\sigma^2_{\ln c_u} = \gamma(D) \ln\left(1 + \frac{\sigma^2_{c_u}}{\mu^2_{c_u}}\right) \tag{20}$$

Eq. (5*a*) is used in Eq. (20). For an exponential correlation function [Eq. (6)] that is separable in the vertical direction, the variance reduction function $\gamma(D)$ also is separable in the vertical direction and can be expressed as

$$\gamma(D) = \gamma(L_x, L_y, L_z) = \gamma(L_z) \times \gamma(L_x, L_y) \tag{21}$$

where $\gamma(L_z)$ is given analytically as

$$\gamma(L_z) = \frac{1}{2}\left(\frac{\theta^v_{\ln c_u}}{L_z}\right)^2 \left[\frac{2L_z}{\theta^v_{\ln c_u}} + \exp\left(-\frac{2L_z}{\theta^v_{\ln c_u}}\right) - 1\right] \tag{22}$$

and $\gamma(L_x, L_y)$ can be approximated as

$$\gamma(L_x, L_y) = \frac{1}{2}[\gamma(L_x)\gamma_x(L_y) + \gamma(L_y)\gamma_y(L_x)] \tag{23}$$

for the horizontally isotropic radial correlation part (Vanmarcke 1983).

The variance reduction functions $\gamma(L_x)$ and $\gamma_x(L_y)$ in Eq. (23) are defined as follows (Fenton and Griffiths 1993, 2002):

$$\gamma(L_x) = \left[1 + \left(\frac{L_x}{\theta^h_{\ln c_u}}\right)^{3/2}\right]^{-2/3} \tag{24}$$

$$\gamma_x(L_y) = \left[1 + \left(\frac{L_y}{\theta^y_x}\right)^{3/2}\right]^{-2/3} \tag{25}$$

$$\theta^y_x = \theta^h_{\ln c_u}\left[\frac{\pi}{2} + \left(1 - \frac{\pi}{2}\right)\exp\left(-\frac{L_x^2}{(\pi/2)^2(\theta^h_{\ln c_u})^2}\right)\right] \tag{26}$$

Similar equations can be expressed for $\gamma(L_y)$ and $\gamma_y(L_x)$ using a similar expression for θ^x_y; that is, by simply changing the subscripts and superscripts in Eqs. (24)–(26) from x to y and from y to x.

Alternatively, $\gamma(D)$ can also be obtained from numerical integration of the correlation function [Eq. (6)], for example, by Gauss–Legendre quadrature (Fenton and Griffiths 2008).

Statistical Moments of M_c

With reference to Eq. (9), $\bar{c}_u$ follows a log-normal distribution. Thus, by using the generic inverse transformations of Eq. (5) (i.e., replacing c_u with $\bar{c}_u$ and $\ln c_u$ with $\ln \bar{c}_u$) and Eqs. (14), (19) and (5), the first two moments of $\bar{c}_u$ are

$$\mu_{\bar{c}_u} = \exp\left(\mu_{\ln \bar{c}_u} + \frac{1}{2}\sigma^2_{\ln \bar{c}_u}\right) = \mu_{c_u} \times \frac{1}{(1 + v_c^2)^{[1-\gamma(D)]/2}} \tag{27}$$

and

$$\sigma_{\bar{c}_u} = \sqrt{\exp(\sigma^2_{\ln \bar{c}_u}) - 1} \times \mu_{\bar{c}_u} = \sqrt{(1 + v_c^2)^{\gamma(D)} - 1} \times \mu_{c_u} \times \frac{1}{(1 + v_c^2)^{[1-\gamma(D)]/2}} \tag{28}$$

Taking expectations of Eq. (11) leads to

$$\mu_{M_c} = \frac{\mu_{q_f}}{\mu_{c_u}} = \frac{\mu_{\bar{c}_u} \times N_c'}{\mu_{c_u}} \tag{29}$$

Eq. (27) indicates the following:

$$\mu_{\bar{c}_u} = \mu_{c_u} \times \frac{1}{(1 + v_c^2)^{[1-\gamma(D)]/2}} \overset{\gamma(D)\to 0}{\rightarrow} m_{c_u} = \mu_{c_u} \times \frac{1}{(1 + v_c^2)^{1/2}} \tag{30}$$

where m_{c_u} = median of c_u. Moreover, for $0 \le \gamma(D) \le 1.0$, the following holds:

$$\mu_{c_u} \times \frac{1}{(1+v_c^2)^{[1-\gamma(D)]/2}} \ge \mu_{c_u} \times \frac{1}{(1+v_c^2)^{1/2}} \tag{31}$$

In other words, $\mu_{\bar{c}_u} \ge m_{c_u}$, and μ_{q_f} decreases toward $m_{c_u} N_c'$ {i.e., the q_f value based on the median [Eq. (11)]} as $\gamma(D)$ approaches 0 [or μ_{M_c} decreases toward $(m_{c_u} N_c')/\mu_{c_u}$, the M_c value based on the median]. This means that for the same domain D, as $\theta_{\ln c_u}$ decreases and thereby $\gamma(D)$ becomes smaller, the mean bearing capacity μ_{q_f} (or mean bearing capacity factor μ_{M_c}) approaches the bearing capacity q_f (or bearing capacity factor M_c) based on the median of c_u. Conversely, when $\gamma(D)$ approaches 1.0 ($\theta_{\ln c_u}$ goes to infinity), μ_{q_f} increases toward $\mu_{c_u} N_c'$ (i.e., the q_f value based on the mean).

Eq. (17) is equivalent to taking $\bar{c}_u$ as the median (i.e., $\mu_{c_u}/\sqrt{1+v_c^2}$) in Eq. (11); that is, the prediction equation for $\mu_{\ln M_c}$ coincides with $\mu_{\ln M_c}$ based on the median.

According to Eq. (11), the standard deviation of M_c is

$$\sigma_{M_c} = \frac{\sigma_{q_f}}{\mu_{c_u}} = \frac{\sigma_{\bar{c}_u} \times N_c'}{\mu_{c_u}} \tag{32}$$

where $\sigma_{\bar{c}_u}$ is given in Eq. (28).

Probability of Failure

Based on Eqs. (17) and (20), the probability of a design failure (p_f) for a certain factor of safety F relative to the deterministic q_f, q_f^d, based on the mean μ_{c_u} may be defined as

$$p_f = P\left[q_f \le \frac{q_f^d}{F}\right] = P\left[\frac{q_f}{\mu_{c_u}} \le \frac{N_c'}{F}\right] = P\left[M_c \le \frac{N_c'}{F}\right]$$
$$= P\left[\ln M_c \le \ln \frac{N_c'}{F}\right] = \Phi\left(\frac{\ln \frac{N_c'}{F} - \mu_{\ln M_c}}{\sigma_{\ln M_c}}\right) \tag{33}$$

where Φ = cumulative standard normal distribution function; and $q_f^d = \mu_{c_u} N_c'$.

No variation of footing load was considered in this paper; the probability of failure is defined as the probability of the bearing capacity of a varying soil being smaller than the deterministic bearing capacity based on the mean property value divided by some factor of safety (which gives the allowable bearing capacity, i.e., $q_f^a = q_f^d/F$).

Finite-Element Model

A viscoplastic finite-element program was written, based on Smith and Griffiths (2005), to carry out the bearing capacity analysis of a rough rigid square footing founded on a weightless soil with spatially varying shear strength parameter c_u. The algorithm performs iterative plastic stress redistribution by using an elastic-perfectly plastic stress–strain relationship with a Tresca failure criterion.

The finite-element program has three input parameters: Young's modulus E, Poisson's ratio ν, and undrained shear strength c_u. In this study, c_u was treated as a random field, whereas E and ν were kept constant (i.e., $E = 100{,}000$ kN/m^2, and $\nu = 0.3$) because their values do not significantly affecting the ultimate bearing capacity (Li et al. 2020). The E values were chosen such that E/μ_{c_u} fell in the range 100–1,500 (Bowles 1996). Although an undrained analysis implies a Poisson's ratio of 0.5, the smaller value (i.e., 0.3) used in this paper aids numerical stability and efficiency, without affecting the computed bearing capacity (Li 2017). The bearing capacity is computed based on the sum of nodal reaction forces Q_f using the converged stress field; convergence is defined as the point at which the sum of the nodal reactions levels out within a relative error tolerance of 0.0001. The bearing capacity then is computed as

$$q_f = Q_f/BL \tag{34}$$

where B and L = footing width and length, respectively. In the case of square footings, $L = B$.

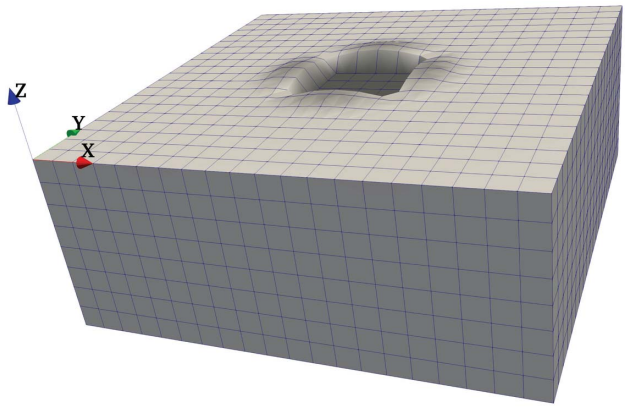

Fig. 2. Deformed finite-element mesh (with example deformations enlarged by a factor of 3) for square footings.

Fig. 2 shows the 3D finite-element mesh discretization used in the following analyses, relative to a Cartesian (i.e., x, y, z) coordinate system. The mesh comprises 3,200 14-node hexahedral elements ($20 \times 20 \times 8$). Each element has dimensions of 0.25×0.25 m in plan and 0.25 m in depth. Thus, the problem domain has a size of $5 \times 5 \times 2$ m. The footing width considered is $B = 1.0$ m. The finite-element analysis domain size used for $B = 1.0$ m has been shown to be sufficiently large to avoid significant boundary effects (Li et al. 2020). The boundary conditions are a fixed base, and rollers on the two x–z (front and back) and two y–z (left and right) faces preventing displacement perpendicular to the faces. The rough footing conditions are simulated by restraining horizontal displacements (i.e., in the x- and y-directions) of the nodes representing the footing.

Deterministic Finite-Element Analysis

Deterministic FEA was carried out with the mean undrained shear strength, $\mu_{c_u} = 100$ kPa, and COV $v_c = 0$. Various finite-element sizes (by varying the number of elements discretizing the problem domain) and types (14-node or 20-node) first were used to investigate the influence of mesh density and element type. The calculated bearing capacity factors (N_c') and required running time for a rough rigid footing are listed in Table 1 for various combinations. The results of analyses with the 14-node elements were virtually identical to those with the 20-node elements. Furthermore, results using finer meshes were closer to the theoretical solution of 1.2×5.14 (Meyerhof 1951) (this theoretical value was based on circular footings, because no theoretical solutions for square footings are available). An improved agreement between the computed and theoretical solution can be obtained by using even finer meshes. However, the computational cost then increases substantially. To run the following (Monte Carlo) analyses in a reasonable time, the coarse mesh with 14-node elements was used in this study. (Using the finer mesh would have required 1 month to run 200 realizations serially on a single CPU for a given combination of

Table 1. Bearing capacity factors and CPU timings for deterministic finite-element analyses with different element sizes and types

Number of elements in x- or y-direction	Element type	CPU time	N_c'
40	20-node	7 h	6.546
40	14-node	3.5 h	6.517
20	20-node	12 min	7.262
20	14-node	8 min	7.389

SOF and COV; hence, the total time for the following 6×7 cases would have been infeasible.)

The bearing capacity factor $N_c' = 7.389$ obtained using the coarse mesh was too crude an approximation (it should be 6.17). To take account of the discretization error in the following Monte Carlo investigation, the calculated bearing capacity factors $\{M_c$ [Eq. (35)]$\}$ using the crude mesh were normalized by the corresponding finite-element deterministic values of 7.389 and then scaled to bearing capacity factors relative to 6.517 (i.e., the deterministic value N_c' based on the finer mesh); $N_c' = 6.517$ is very close to the theoretical value of 6.168 and was considered to be acceptable, with a relative error of 5.6%. This normalization and scaling procedure was based on Li et al. (2020), who ran MC simulations for both coarse and finer meshes and observed that $M_c^1/N_c'^1 \approx M_c^2/N_c'^2$ (where 1 and 2 represent FE discretization levels) for typical scenarios of spatial variability (i.e., typical values of SOF representing small, medium, and large scale variability) and COV = 0.2. This also was observed herein for COV = 0.5, i.e., the higher end of the COV range of practical interest. With this procedure, costly MC simulations based on the fine mesh for various cases were avoided by scaling the results (by a factor of 6.517/7.389) based on the coarse mesh. In this case, $N_c'^1 = 7.389$ and $N_c'^2 = 6.517$, and the random M_c^1 values were the series of MC simulation results based on the coarse mesh. Therefore, the MC simulation directly calculated M_c^1 results based on the coarse mesh and these values then were scaled to a series of values that closely approximated M_c^2, the MC results of the finer mesh. This procedure made this study feasible while maintaining relatively good accuracy.

Monte Carlo Simulation versus Theoretical Predictions

The finite-element and random field models previously introduced were combined (i.e., by mapping random field values to the $2 \times 2 \times 2$ Gaussian points within each finite element) within a Monte Carlo simulation framework, a form of analysis sometimes referred to as the random finite-element method (RFEM) (Fenton and Griffiths 2008), to carry out the parametric studies in the following sections. Table 2 lists the input parameters for the Monte Carlo simulations. The values of COV, v_c, were chosen based on the recommended range of 0.1–0.5 for clays (Lee et al. 1983; Hicks and Samy 2002; Li 2017). This range is based on databases (e.g., Phoon and Kulhawy 1999) from geotechnical site investigations (i.e., from which a statistical analysis can be made to separate the COV due to soil spatial variability from the COV due to insufficient information or limited intensity, usually called statistical uncertainty). However, it is argued that larger COVs also may be possible in view of the difficulty in separating the two COVs without further site investigations (which is likely to be the case for any new design). Therefore, some higher COVs also were assumed in this study. In order for the COVs from a large database to be realistic, staged site investigation data must be analyzed to separate COVs due to statistical errors from COVs due to inherent soil spatial variability.

Table 2. Input parameters used in Monte Carlo simulations

Parameter	Value
μ_{c_u} (kPa)	100
v_c	0.1, 0.2, 0.5, 1.0, 2.0, 5.0
$\theta_{\ln c_u}$ (m)	0.1, 0.5, 1.0, 2.0, 4.0, 8.0, 50

The values of the scale of fluctuation of clay soils were chosen based on a comprehensive literature review (Li 2017), which reported various SOF values for the c_u of clay soils. Due to geological deposition, the SOF in the horizontal direction generally is larger than the SOF in the vertical direction. Although the analysis models in this paper are capable of simulating anisotropically correlated random fields, the following results are presented only for the case of isotropic heterogeneity. Site-specific anisotropy is left for later work.

Based on the SOF values in the literature, seven cases (Table 2) for the scale of fluctuation $\theta_{\ln c_u}$ were investigated [$\theta_{\ln c_u}$ is not much different in magnitude from θ_{c_u} for practical ranges of COV (Griffiths and Fenton 2001; Popescu 2004; Fenton and Griffiths 2004)]. Each MC simulation involved the generation of N realizations of the shear strength random fields and the subsequent nonlinear finite-element analysis of the bearing capacity. The bearing capacity for each realization was different due to different (relative) spatial distributions of strong and weak soil elements. For each realization, a stochastic bearing capacity factor, nondimensionalized with respect to the mean undrained shear strength μ_{c_u}, is given by

$$M_c^i = q_f^i/\mu_{c_u}, \quad i = 1, 2, \ldots, N \tag{35}$$

where superscript i denotes realization number; and $N = 200$ = number of realizations. For $N = 200$, the standard error for the estimate of the mean of M_c is $\sqrt{1/N}\sigma_{M_c} = 0.07\sigma_{M_c}$ and the standard error for the estimate of the variance of M_c is $\sqrt{2/N}\sigma_{M_c}^2 = 0.10\sigma_{M_c}^2$.

More realizations are needed to obtain a probability distribution of M_c with more confidence. The standard deviation of the probability of failure p_f is approximately $\sqrt{p_f(1-p_f)/N}$. For $p_f =$ 5% and $N = 200$, $\sigma_{p_f} \approx 1.5\%$, which is not a particularly small standard error. However, because three-dimensional nonlinear analysis is very time consuming (El Haj et al. 2019), the number of realizations selected was deemed sufficient to analyze typical trends and draw general conclusions in three dimensions. As a compromise, the RFEM simulation results were not directly used to estimate p_f; instead, the fitted distribution parameters were used to calculate the failure probabilities from the simulations, assuming that the distribution of M_c continues to be modeled by the fitted distribution at the tails (Fenton and Griffiths 2008). Other alternatives include the use of an estimator variance reduction technique such as subset simulation combined with random fields (Ahmed and Soubra 2012; van den Eijnden and Hicks 2017), and the development of efficient approximate analytical formulations, which was precisely the goal of this study.

Variability of Bearing Capacity

A square footing with $L = B = 1.0$ m, resting at the center of the problem domain, was investigated based on an ensemble of random field realizations. Based on the previously mentioned normalization and scaling procedure, Fig. 3 presents the probability distributions from RFEM simulations for $\theta_{\ln c_u} = 2.0$ m, for both COV = 0.1 and 1.0. The fitted log-normal and predicted [Eqs. (17) and (20)] distributions are superimposed on the histograms. The log-normal distribution fit the simulated results quite well, with encouraging

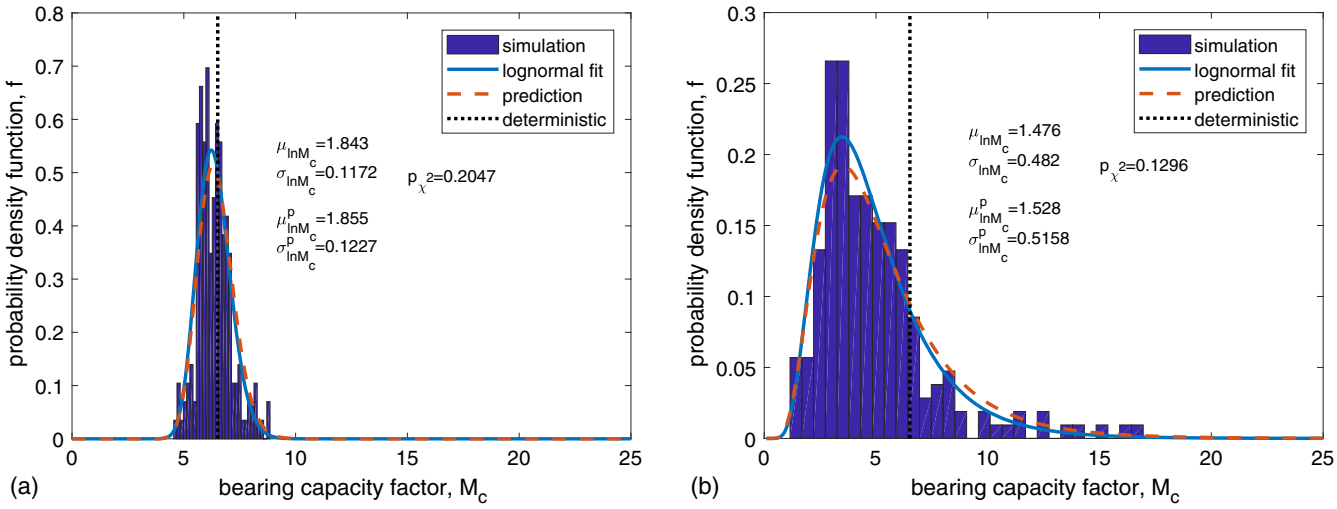

Fig. 3. Frequency distributions from RFEM simulations with fitted log-normal and predicted distributions ($\theta_{\ln c_u} = 2.0$ m, and $N = 200$) (after scaling to finer mesh): (a) COV = 0.2; and (b) COV = 1.0.

chi-squared goodness test p-values (i.e., large p-values support the null hypothesis that the M_c distribution is approximated closely by the log-normal distribution), and the predicted distribution also was quite close to the fitted distribution. The FE deterministic value of 6.517 also is shown in Fig. 3. In the two cases [Figs. 3(a and b)], the mean bearing capacity factor $\mu_{M_c} = 6.361$ and 4.932, respectively, both of which were smaller than the deterministic value of $N_c' = 6.517$ due to the effect of spatial variability that promotes failure surfaces along the weakest and shortest path. The smaller value of 4.932 was expected for a larger COV of 1.0, as is shown in the section "Mean and Variance of Bearing Capacity" (Fig. 7).

Fig. 4 shows an example bearing failure of a square footing on the soil mass with a spatially varying soil property [i.e., Fig. 1(b), in which the square footing is represented by a square on the top surface], computed based on the finer 40-element mesh ($40 \times 40 \times 16$). The weaker (lighter) soil on the left side of the footing [Fig. 1(b)] triggered a nonsymmetric failure mechanism, and the failure surface only approximately followed a log spiral (i.e., the RFEM sought the path of least resistance).

Mean and Variance of Bearing Capacity

Before comparing the two predicted moments of bearing capacity with those directly calculated from the RFEM simulations, an averaging domain size needs to be etermined. A size of $D = w \times 5w$, where w is the active wedge zone depth $(B/2)\tan(\pi/4 + \phi/2)$ for the strip footing bearing failure mechanism, was recommended in the 2D analysis of Fenton and Griffiths (2003). Hence, for a frictionless soil, $w = B/2$. Honjo and Otake (2013) recommended an averaging domain of $D = 0.7B \times 2B$ (Ching et al. 2015), i.e., $D = 1.4w \times 4w$, in their analysis of cohesive soils, although they suggested a larger domain for cohesionless soils based on areas directly below the footing within the slip lines. For cohesive-frictional soils, they suggested that the averaging domain should be the same as that for cohesionless soils (Honjo and Otake 2013). In terms of the volumes involved, the two cited studies are similar. For cohesive soils in this study, an area of $D = w \times 4w \times 4w$ was used unless stated otherwise. This is discussed further in the "Probability of Failure" section.

Fig. 5(a) shows the mean bearing capacity from the RFEM simulations and the corresponding predicted solution based on the theoretical equations, for various values of COV. For both small enough SOF and large enough SOF, the simulation results tend toward the prediction results. The simulation deviated from the prediction for high COVs because of a valley–hill behavior (which is explained subsequently) as $\theta_{\ln c_u}$ decreased from 50 to 0.1 m, which the theoretical model is not able to capture because it does not consider the inherent mechanical stress–strain mechanism that governs the failure together with random variation (whereas the RFEM simulation is perfectly capable of doing so). Fig. 5(b) shows the results

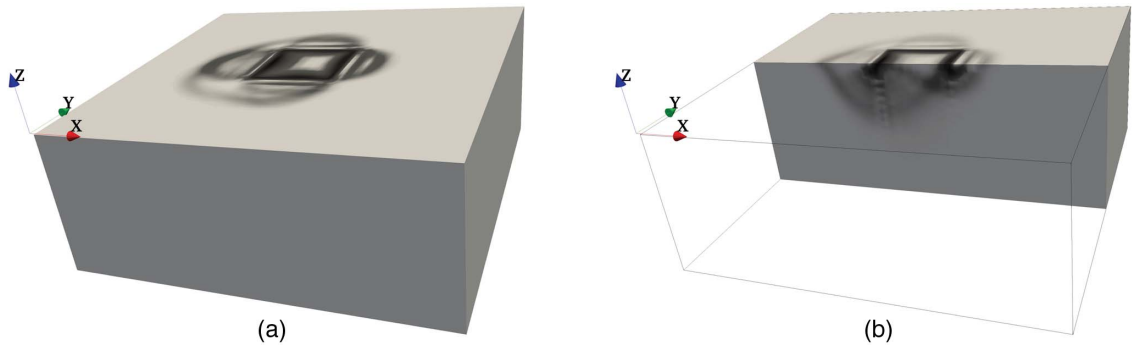

Fig. 4. An example failure mechanism (in terms of shear strain invariant) for the square footing on a spatially varying soil ($\theta_{\ln c_u} = 2.0$ m) with COV = 0.2: (a) entire domain; and (b) domain cut.

J. Geotech. Geoenviron. Eng., 2021, 147(6): 04021035

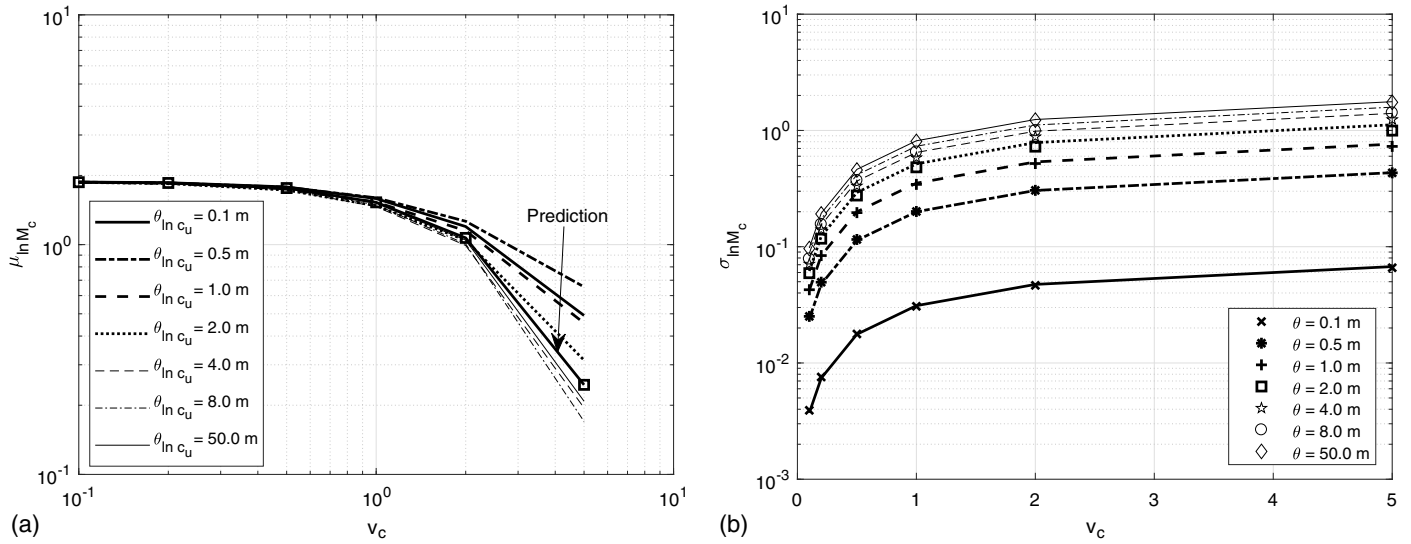

Fig. 5. Simulated and predicted mean and standard deviation of $\ln M_c$: (a) $\mu_{\ln M_c}$ versus COV for various $\theta_{\ln c_u}$ (line with square markers represents prediction); and (b) $\sigma_{\ln M_c}$ versus COV for various $\theta_{\ln c_u}$ (lines represent prediction, and various marker points represent RFEM simulation; subscripts omitted for $\theta_{\ln c_u}$ due to limited space).

for $\sigma_{\ln M_c}$, demonstrating that the predictions remarkably matched the simulation results. In spite of the simplification regarding the mechanical part, the theoretical model provides good results (i.e., mean and variance) for parameters of practical interest (i.e., COVs from 0.1 to 1.0).

Figs. 6(a and b) show the simulated $\mu_{\ln M_c}$ as a function of SOF; the horizontal lines are the predictions based on Eq. (17), which is a function of COV {the vertical axis scales in the two sub-figures indicate that as COV increases, $\mu_{\ln M_c}$ decreases [Fig. 5(a)]}. When SOF is small enough, $\mu_{\ln M_c}$ is equivalent to running a single analysis based on the median of c_u and taking $\ln \bar{c}_u$ as $\mu_{\ln \bar{c}_u}$ in Eq. (13)—i.e., in Eq. (9), when SOF is small, $\bar{S}^a$ has negligible variance and $\mathrm{E}[\bar{S}^a] = 0$, so that for any realization, $\bar{S}^a \approx 0$, which makes $\bar{c}_u \approx \exp(\mu_{\ln c_u})$, i.e., the median. When SOF is large enough, $\mu_{\ln M_c}$ is equivalent to running a series of analyses, each based on a single value of c_u (i.e., within each realization) that is random from realization to realization, and taking the average of $\ln \bar{c}_u$ across realizations in Eq. (13) [in this case, the $\ln c_u(\boldsymbol{x_i})$ values ($i = 1, \ldots, n$) in Eq. (9) are the same for the n different locations within each realization; i.e., $\bar{c}_u = c_u^j$ for realization j, so that $\mu_{\ln \bar{c}_u}$ is taken across the realizations].

For the RFEM simulations, $\mu_{\ln M_c}$ is a function of SOF. The simulated valley–hill behavior of $\mu_{\ln M_c}$ versus $\theta_{\ln c_u}$ as SOF decreases may be better explained by the behavior of μ_{M_c} versus $\theta_{\ln c_u}$ [Figs. 7(a and b)], where μ_{M_c} is theoretically a function of SOF [Eqs. (27) and (29)]. That is, the two moments of $\ln M_c$ are related to those of M_c by log-normal transformation equations [Eq. (5)]. This also applies to $\ln q_f$ and q_f, because $\ln q_f$ and $\ln M_c$ differ only by a constant $\ln \mu_{c_u}$ [Eqs. (7) and (12)], and M_c and q_f differ by a constant ratio μ_{c_u} [Eq. (11)].

Theoretically, the $\mu_{\ln M_c}$ or $\mu_{\ln q_f}$ prediction is constant for any given COV [Eq. (17)], and is not a function of SOF [i.e., a

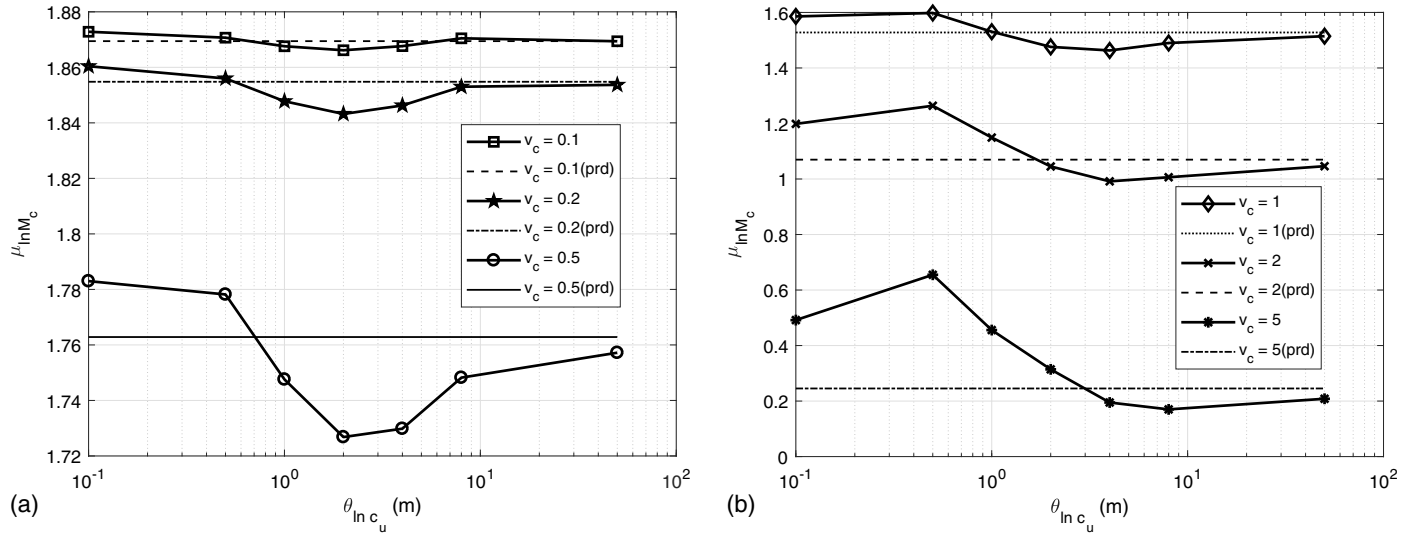

Fig. 6. $\mu_{\ln M_c}$ versus $\theta_{\ln c_u}$ for: (a) COV = 0.1, 0.2, and 0.5; and (b) COV = 1.0, 2.0, and 5.0. prd indicates prediction.

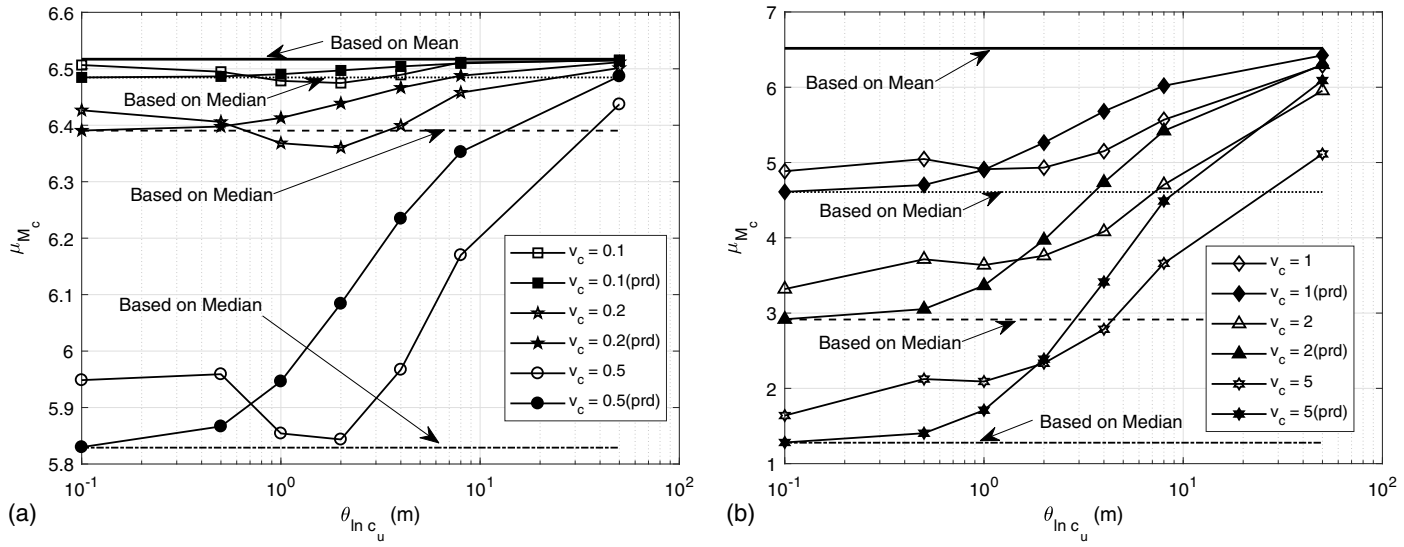

Fig. 7. μ_{M_c} versus $\theta_{\ln c_u}$ for: (a) COV = 0.1, 0.2, and 0.5; and (b) COV = 1.0, 2.0, and 5.0. Lower and upper bounds (based on median and mean, respectively) indicated as lines without markers; and prd indicates prediction.

horizontal line in Figs. 6(a and b)]. However, the theoretical prediction of μ_{M_c} or μ_{q_f} is a function of SOF [Eqs. (27) and (29); Figs. 7(a and b)], and there are associated lower and upper bounds when SOF approaches 0 or infinity. This is because the variance of $\ln M_c$ or $\ln q_f$ comes into play when evaluating the mean of M_c or q_f [e.g., the inverse of Eq. (5) when considering the generic transformations for any log-normally distributed variable] and the variance of $\ln M_c$ or $\ln q_f$ is related to the variance function which is a function of SOF and domain size D [Eq. (20)].

Figs. 7(a and b) show the RFEM simulated μ_{M_c} versus $\theta_{\ln c_u}$ for various COVs and the predictions based on theory [Eqs. (27)–(29)], together with their respective theoretical lower and upper bounds (i.e., based on the median and mean, respectively). The valley–hill behavior in the RFEM simulation may be noted when $\theta_{\ln c_u}$ decreased from 50 to 0.1 m, especially for larger values of COV. For small COV, the simulated results are expected to decrease to results based on the median if an even smaller SOF is used.

The theoretical solution does not take account of the valley mean bearing capacity behavior for intermediate values of $\theta_{\ln c_u}$; it continuously decreases as $\theta_{\ln c_u}$ decreases. In contrast, the valley occurred in the finite-element simulations due to the weakest path mechanistic effect in the RFEM simulations. Therefore, without disobeying the theoretical trend as $\theta_{\ln c_u}$ decreases, a small hill (after the valley) must appear in the simulated results before it continues to decrease toward the theoretical lower bound (i.e., the value based on the median). This valley value may be smaller or larger than the value based on the median, and only in the former case can it be called a worst case in which μ_{M_c} reaches a minimum.

Fenton and Griffiths (2003) also observed a valley behavior in their 2D analyses, but they did not observe a hill followed by a further reduction in μ_{M_c} as the SOF decreased. This is believed to be due to the larger variance reduction in three dimensions than in two dimensions [i.e., Eq. (21), which has an additional term in three dimensions compared with two dimensions]; i.e., in the 2D study, the $\gamma(D)$ term in Eq. (30) is not small enough to drive μ_{M_c} down to the value based on the median through Eq. (29).

Although the theoretical predictions of μ_{M_c} for large COV were not particularly good, the predictions for practical ranges of COV (i.e., in the range 0.1–0.5) were quite good [Figs. 6(a) and 7(a); note the change in vertical axis scales].

Probability of Failure

This paper is intended for the reliability-based design of footings targeting some acceptable failure probability, and, when evaluating the failure probability, both the mean and variance of $\ln q_f$ or $\ln M_c$ come into Eq. (33); hence, the statistics of $\ln q_f$ or $\ln M_c$ then are directly relevant.

Fig. 8 shows the simulated probability of failure [based on Eq. (33), with the first two moments calculated directly from Eqs. (35) and (34)] versus the predicted probabilities of failure [based on Eq. (33), with the two moments predicted using theoretical equations] for various SOFs and COVs using an averaging domain of $w \times 5w \times 5w$; the 95% confidence interval also is plotted (dotted lines). Although most of the points lie within the 95% confidence interval, some predictions are on the unconservative side, i.e., predicted p_f smaller than simulated p_f. This was because the variance predictions for $\ln M_c$ when using $D = w \times 5w \times 5w$ were smaller than the simulated variance, whereas the mean predictions for $\ln M_c$ did not change (i.e., they were not related to D). The results in Fig. 8 are based on F [Eq. (33)] increasing from the upper right corner to the lower left corner.

To attempt to improve the theoretical prediction, a smaller domain of $D = w \times 4w \times 4w$ also has been used, i.e., to increase the prediction variance (a smaller domain means less variance reduction) and thus increase the predicted p_f and reduce the degree of unconservatism (Fig. 9). The points in Fig. 9 are less disperse; they lie more closely within the 95% confidence interval and mainly lie on the conservative side, i.e., the predicted p_f is slightly larger than the simulated value in most cases. The agreement between the simulation and prediction is very good for COVs of practical interest, but not very good for high COVs (not shown). This is to be expected, because the probability predictions are only as good as the predictions of the two moments presented previously—i.e., the prediction of $\mu_{\ln M_c}$ is not very good for high COVs [Fig. 5(a)]. For COVs of concern in practice, the case of $\theta_{\ln c_u} =$ 0.1 m was overly conservative, largely due to the underpredicted mean [Figs. 6(a and b)]. This is an exceptional case in which the larger averaging domain ($w \times 5w \times 5w$) may predict a better p_f, i.e., the values of p_f are not too conservative (Figs. 8 and 9). The underprediction of the variance (when using $w \times 5w \times 5w$), combined with the underprediction of the mean for this particular

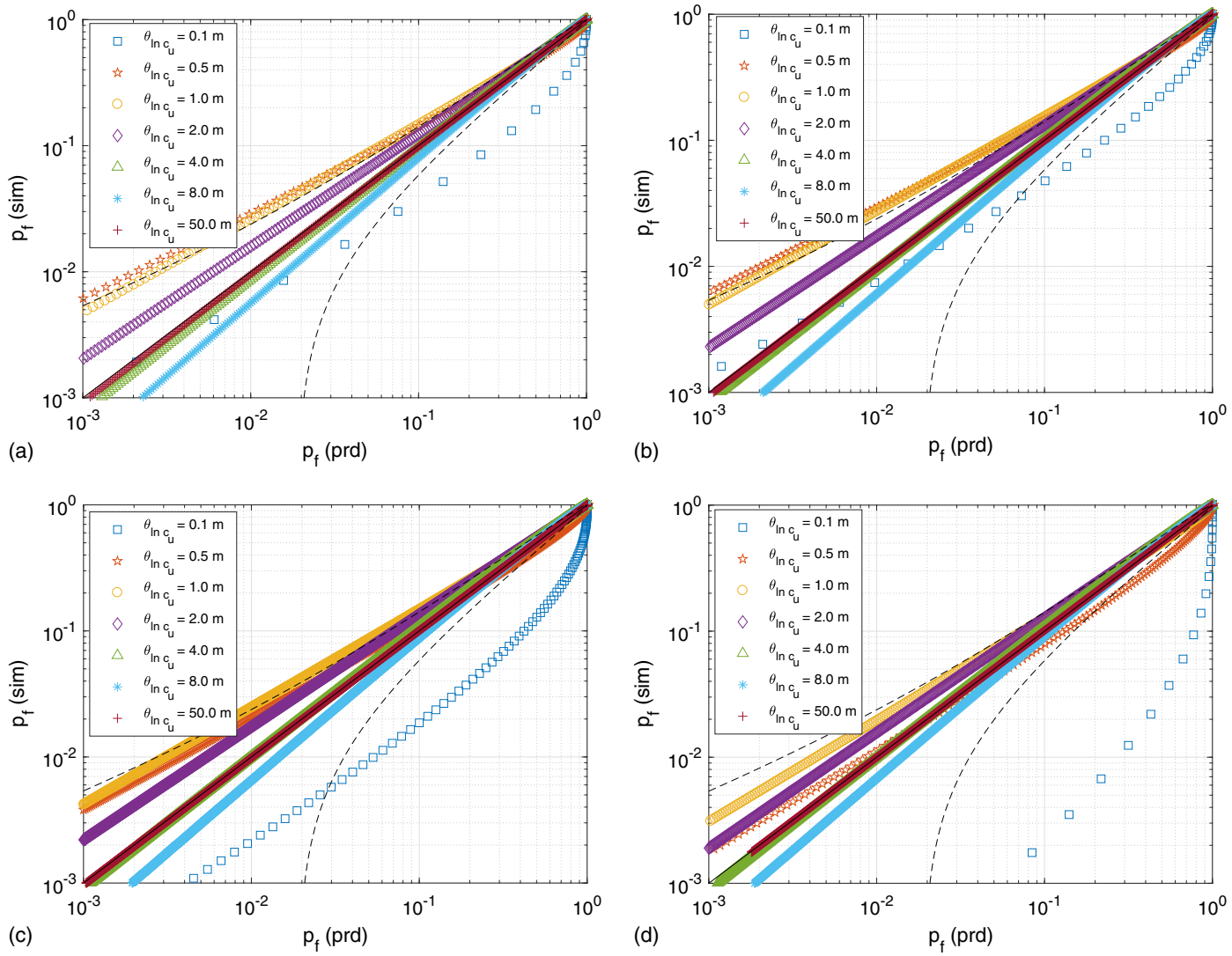

Fig. 8. Predicted (prd) versus simulated (sim) probabilities of failure for different values of the scale of fluctuation, with averging domain size $w \times 5w \times 5w$: (a) COV = 0.1; (b) COV = 0.2; (c) COV = 0.5; and (d) COV = 1. Dotted lines indicate the 95% confidence interval.

value of SOF = 0.1 m, caused the overpredicted p_f to be less conservative or even slightly unconservative [Figs. 8(b) and 9(b)]. Intuitively, for higher COVs, the probability prediction for $\theta_{\ln c_u} = 0.5$ m should be worse than for $\theta_{\ln c_u} = 0.1$ m, because the corresponding $\mu_{\ln M_c}$ prediction is worse [Fig. 6(b)]; however, Fig. 9 shows the opposite. This is because the small $\theta_{\ln c_u}$ value of 0.1 m yields the smallest $\sigma_{\ln M_c}$, which in turn implies a rapidly increasing cumulative distribution of $\ln M_c$ over a small range. Thus, slight errors in the estimate of $\mu_{\ln M_c}$ yield large errors in the probability prediction.

The use of $w = B/2$ for frictionless soil, as mentioned previously, was based on the active wedge zone depth in the failure mechanism. It may be argued that the influence zone depth may be slightly larger than the active wedge zone depth due to the presence of the log-spiral zone. On the other hand, the actual volume of soils resisting the bearing failure along the failure surfaces (i.e., the volume of soil involving plastic deformation) may be smaller than the failure region enveloped in the failure surface (and therefore a smaller horizontal dimension may be applicable). Therefore, averaging domains of $D = 1.5w \times 4w \times 4w$ and $1.5w \times 3w \times 3w$ also were studied. The results of $D = 1.5w \times 4w \times 4w$ had somewhat more-unconservative values of p_f than those of $D = w \times 4w \times 4w$ due to the larger averaging domain (i.e., smaller prediction variance). The results of $D = 1.5w \times 3w \times 3w$, on the other hand, had more-conservative predictions of p_f than those of $D = w \times 4w \times 4w$. Just as Fig. 8 shows predictions that are too much on the unconservative side, Fig. 10 shows the other end of the prediction spectrum (i.e., predictions that are too conservative). Overall, other averaging domain sizes (by trial and error) did not provide better results than those in Fig. 9.

A fixed averaging domain was used in this paper, and the results of using $w \times 4w \times 4w$ were satisfactory for practical values of COVs. Comparing Figs. 8 and 9, however, indicated that an averaging domain of $w \times 5w \times 5w$ may be better for small and large values of SOF. This is somewhat to be expected, because for small or large values of SOF, the failure mechanism is approaching the deterministic failure surfaces, based on which the domain of $w \times 5w \times 5w$ was chosen in the first place. For intermediate values of SOF, the smaller domain of $w \times 4w \times 4w$ is better.

Figs. 8–10 are useful for examining the validity of the theoretical prediction equations in this study. However, to use these figures directly for design purposes, it is better to consider the probabilities of failure as functions of the factor of safety F, SOF, and COV. Fig. 11 shows the probability of failure versus F for various

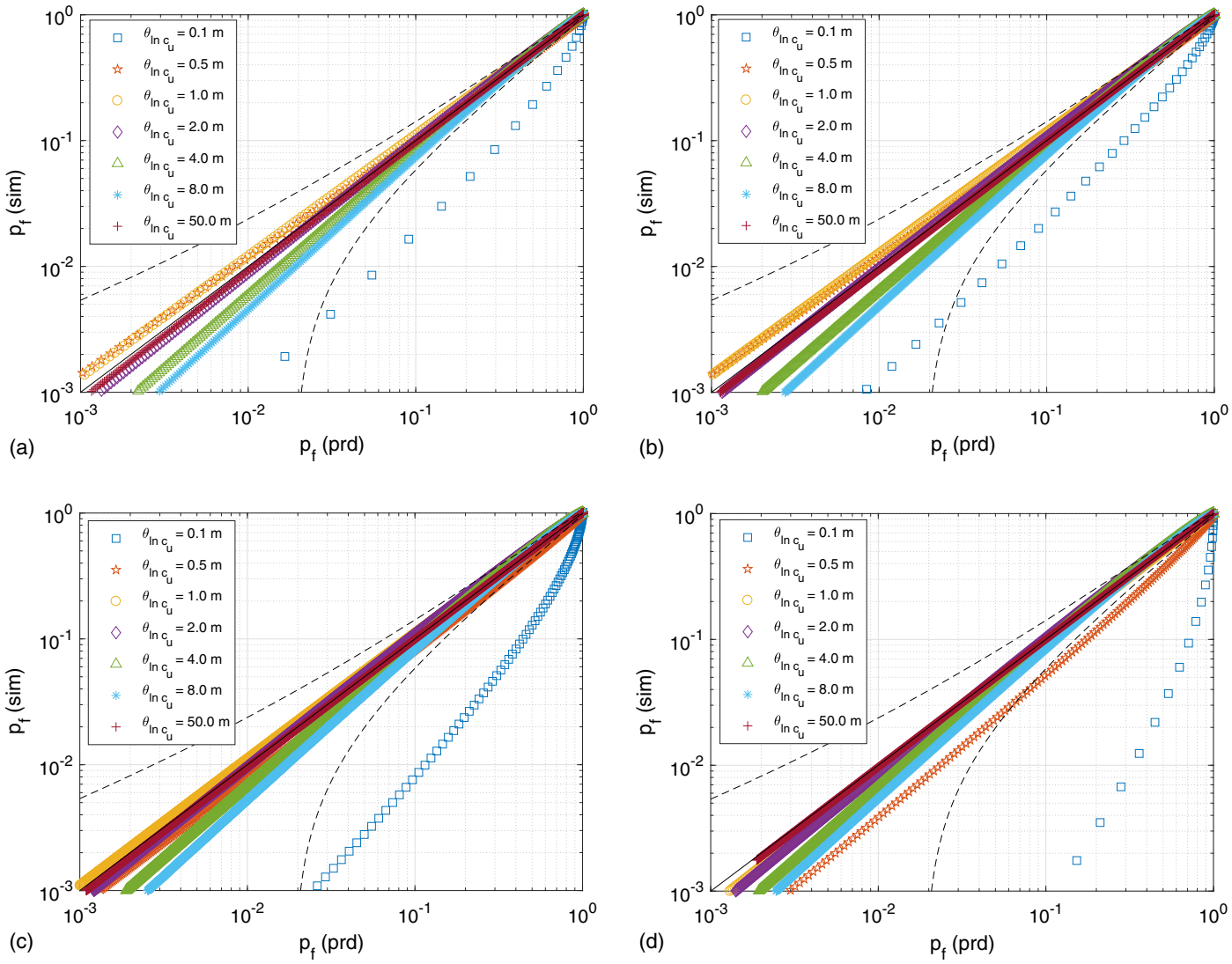

Fig. 9. Predicted (prd) versus simulated (sim) probabilities of failure for different values of the scale of fluctuation, with averging domain size $w \times 4w \times 4w$: (a) COV = 0.1; (b) COV = 0.2; (c) COV = 0.5; and (d) COV = 1. Dotted lines indicate the 95% confidence interval.

SOFs and COV = 0.1 and 0.5, together with the 95% confidence intervals of the simulated probabilities. All predictions agreed quite well with the simulations [the match in Figs. 11(a–d) is remarkably good, with the simulated points overlapping the prediction line], with some predictions being slightly conservative. In cases in which the predictions were slightly conservative [e.g., Figs. 11(e and f)], the predictions still were within the 95% confidence interval of the simulated probabilities. This discrepancy largely may be due to the p_f estimator error in the simulations. That is, more realizations in the simulations are needed to have a smaller σ_{p_f}. In this analysis, the simulation cannot be used for small probabilities less than 0.01 (the coefficient of variation of p_f at this level is $\sqrt{0.01 \times 0.99 \times 200}/0.01 = 0.7$, so for $p_f < 0.01$, the simulation results are not very accurate.).

Limitations and Discussion

Despite the excellent prediction capability of the theoretical equations for practical ranges of COV, this study is not without its limitations, which are as follows:

- The theoretical predictions of bearing capacity variability were validated through comparison with random finite-element simulations. It is assumed that finite-element models can represent closely the behavior of bearing stability under square footings. Although this may not be exactly true, because the true mechanical behavior may never be really known, the assumption seems reasonable at this stage.
- The bearing capacity variability was due purely to soil spatial variability in this study, and not to, e.g., statistical uncertainties arising from limited sampling. In cases in which these two uncertainty sources are not easily separable, it still is assumed that the adopted COV is due only to spatial variability, although high COVs purely due to spatial variability are highly unlikely in practice. Because the basic theory used in this study was local averaging and variance reduction, uncertainty due to other sources was not applicable. However, other uncertainties easily may be superimposed on the variance estimator and any bias factor on the mean estimator.
- The paper focuses on the stochastic behavior of bearing capacity assuming soil heterogeneity with an isotropic correlation structure. However, it is believed that the general theoretical

J. Geotech. Geoenviron. Eng., 2021, 147(6): 04021035

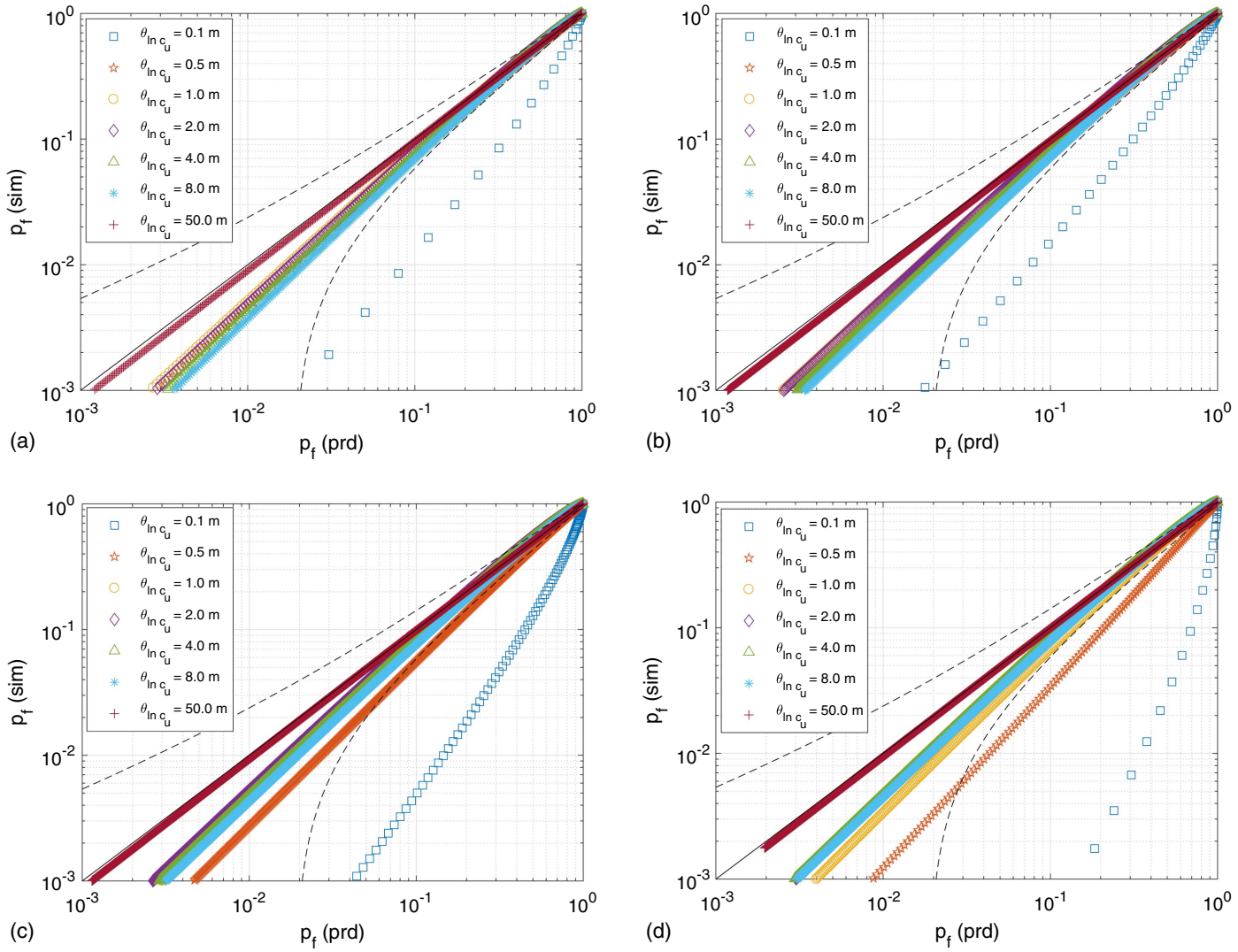

Fig. 10. Predicted (prd) versus simulated (sim) probabilities of failure for different values of the scale of fluctuation, with averging domain size $1.5w \times 3w \times 3w$: (a) COV = 0.1; (b) COV = 0.2; (c) COV = 0.5; and (d) COV = 1. Dotted lines indicate the 95% confidence interval.

solutions also hold for transverse correlation anisotropy, i.e., by using different scales of fluctuation in the three directions or two identical horizontal SOFs and a separate vertical SOF in the variance function. In fact, in this study the averaging domain was taken to be a rectangular domain with a smaller depth to easily accommodate such situations.

- To be analytically tractable, only stationary random fields were considered. For nonstationary random spatial variability, e.g., when a depth trend is present or when the soil is layered, it is possible to calculate numerically the mean and variance of $\bar{c}_u$ from an ensemble of random field realizations. In this case, one still may be able to estimate the mean and variance of the bearing capacity and thus the probability of failure via only random field simulations, without having to run the random finite-element model. The time and computer memory required for random field simulations are substantially less than those for the nonlinear finite-element analysis, and it is feasible to undertake such simulations on standard desktop computers. However, this still needs validation against RFEM analysis. Research in this direction is continuing for overall generality. The situation of multiple soil layers, each with its own statistics, falls into this zonal nonstationarity in general. The aforementioned approach also applies in this case if the layer boundary depth is smaller than the averaging depth w, as long as the failure mechanism passes through all layers. This was discussed further by Bowles (1996) and Kuo et al. (2009).
- Although at most building sites the soil properties at soil sample locations are known, this was not incorporated in the present model. However, conditioning the random field model to be restrained by samples is straightforward and was used in other problems such as slope stability to investigate the influence of sample location and sample intensity (Li et al. 2016b). Although a theoretical model based on conditional random fields is the subject of continuing research, such a model necessarily is more site-specific and is not used easily to make general statements about foundation failure probability (unless every site has the identical sample locations relative to the foundation). Because the effect of known soil data at some distance from the foundation has the main consequence of changing the variance (uncertainty) of the soil properties under the foundation, the results of this paper still can be used by suitably picking the appropriate standard deviation. However, the choice of standard deviation, as a function of the distance to known data, is a topic of future research.

J. Geotech. Geoenviron. Eng., 2021, 147(6): 04021035

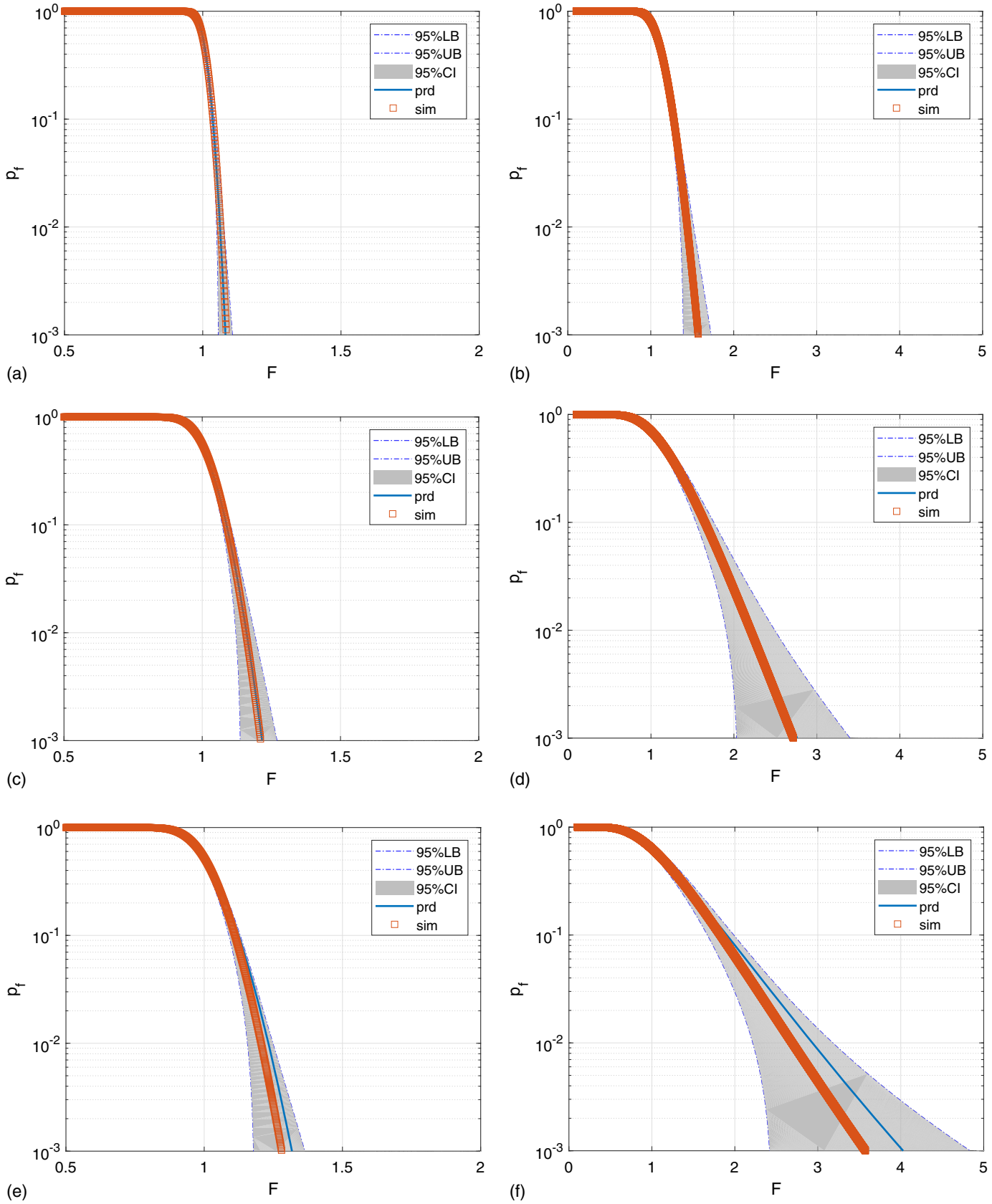

Fig. 11. Predicted (prd) and simulated (sim) probabilities of failure versus F (relative to N_c') for different scales of fluctuation and COVs, with averaging domain size $w \times 4w \times 4w$ (LB denotes lower bound, UB denotes upper bound and CI denotes confidence interval): (a) $\theta_{\ln c_u} = 0.5$ m, and COV $= 0.1$; (b) $\theta_{\ln c_u} = 0.5$ m, and COV $= 0.5$; (c) $\theta_{\ln c_u} = 2$ m, and COV $= 0.1$; (d) $\theta_{\ln c_u} = 2$ m, and COV $= 0.5$; (e) $\theta_{\ln c_u} = 8$ m, and COV $= 0.1$; and (f) $\theta_{\ln c_u} = 8$ m, and COV $= 0.5$.

- A valley–hill behavior of the mean logarithmic bearing capacity was found in the random finite-element simulation, because the method is capable of capturing the weakest link phenomenon at some intermediate value of the scale of fluctuation. In contrast, the prediction of the mean is not capable of capturing this critical valley–hill behavior. Although an empirical modification of the mean is possible based on all the simulation results, this was not pursued because this kind of empirical modification can not readily be considered general, and is possible only through regression analysis of all results from RFEM simulation (perhaps with more MC realizations), which is exactly what this paper strove to avoid.
- Approaches are available to obtain failure probability results without having to run as many simulations as in a crude Monte Carlo simulation. One such approach may be to follow the work of Hu and Ching (2015a), Hu and Ching (2015b) and Ching et al. (2017) by using the independent failure surface concept, but it still requires substantial work with RFEM to calibrate the appropriate number of independent failure surfaces. However, an alternative is to develop a so-called surrogate model (i.e., response surface model) to represent the implicit performance or limit state function (Al-Bittar and Soubra 2013; Al-Bittar et al. 2018; Soubra et al. 2019). These methods include polynomial chaos expansion, kriging-based Monte Carlo simulation, importance sampling, and so on (Al-Bittar and Soubra 2014b; Guo et al. 2019; Guo and Dias 2020). Some of these methods have been used successfully for 2D problems and are finding their way toward 3D applications (El Haj et al. 2019; El Haj and Soubra 2020; Zhou et al. 2020). However, application to 3D problems such as the bearing capacity of square footings in this paper poses a great challenge due to the very high dimensional issue (i.e., $3{,}200 \times 8$ random variables). Because the aim of this paper was to develop a practical method that can be used easily by engineers, the development of a metamodel was beyond the scope of this paper.

Conclusions

The paper investigated the reliability (or probability of failure) with respect to the bearing capacity of square footings on spatially varying purely cohesive soils. Theoretical predictions of the variability of bearing capacity were developed based on local averaging theory and a geometric average model. The analytical predictions of the mean, variance, and probability of failure were found to be in good agreement with RFEM simulations. In both simulations and theoretical predictions, three-dimensional random field models were used to simulate soil spatial variability. In the simulations, 3D finite-element models were used to simulate the bearing failures of rough rigid square footings founded on clay. The results indicated that an equivalent Prandtl equation [Eq. (3)] can be used to predict the two statistical moments and the probability of failure of bearing capacity by using geometric averages of soil properties in the equation.

Based on the current investigation, the following conclusions may be drawn:

1. The degree of spatial averaging or variance reduction is larger in three dimensions than it is in two dimensions, and this helps to explain the different observations for the mean response in three dimensions and two dimensions. In addition, the theoretical derivations help to bound the numerical solutions. However, the weakest path cannot be represented using the theoretical prediction.
2. An averaging domain of $w \times 4w \times 4w$ (where $w = B/2$, i.e., the active wedge zone depth for a frictionless soil) was found to be appropriate for taking the geometric averages under the square footings for the theoretical solution. The size of this domain is particularly relevant for the theoretical variance estimation.
3. The theoretical solution, using a fixed averaging domain size, was shown to provide reasonably accurate predictions for practical ranges of COVs. This is thought to be because the size of the averaging domain is related closely to the mechanical influence domain for bearing capacity problems and dominantly is determined by the traditional Prandtl failure mechanism for a given footing width. However, a larger averaging domain of size $w \times 5w \times 5w$ was found to be slightly better for small and large values of SOFs.
4. The analytical predictions (mean, variance, and probability of failure) based on the theoretical solution can be used satisfactorily for the reliability-based ultimate limit state design of square footings with soil variability parameters of practical interests (i.e., COV < 1.0). Probability of failure graphs (together with confidence intervals) are provided as a function of the traditional factor of safety for various values of COV and SOF (because $B = 1.0$ m in this paper, the probability results generally apply to nondimensionalised SOF$/B$), to facilitate their use by practicing engineers.

Data Availability Statement

Some or all data, models, or code that support the findings of this study are available from the corresponding author upon reasonable request.

Acknowledgments

The first author appreciates the financial support of the National Natural Science Foundation of China (No. 41807228) and the Fundamental Research Funds for the Central Universities (No. 2652019321).

Notation

The following symbols are used in this paper:

B = footing width;
c_u = undrained shear strength;
$\bar{c}_u$ = effective undrained shear strength, i.e., taken as geometric average in this study;
$c_u^j = c_u$ for realization j when SOF is very large;
D = averaging domain size;
E = Young's modulus;
$E[\cdot]$ = expectation operator;
F = factor of safety;
i = element number in discretized averaging domain;
i, j = realization number in Monte Carlo simulations;
L = footing length;
L_a = actual vertical load on footing per unit area;
L_x, L_y, L_z = averaging dimensions in three coordinate directions;
M_c = stochastic bearing capacity factor;
M_c^i = stochastic bearing capacity factor for ith realization;
M_c^1 = stochastic bearing capacity factor for FE discretization level 1;
M_c^2 = stochastic bearing capacity factor for FE discretization level 2;

m_{c_u} = median of c_u;
N = number of Monte Carlo realizations;
N_c = traditional/deterministic bearing capacity factor for strip footing;
N_c' = deterministic bearing capacity factor for square footing;
$N_c'^1$ = deterministic bearing capacity factor for FE discretization level 1;
$N_c'^2$ = deterministic bearing capacity factor for FE discretization level 2;
n = number of non-overlapping rectangular elements below footing;
$P[\cdot]$ = probability of an event;
$p = \chi^2$ goodness of fit test probability;
p_f = probability of failure;
Q_f = sum of nodal reaction forces;
q_f = ultimate bearing stress;
q_f^d = deterministic ultimate bearing stress based on mean property value;
q_f^i = stochastic bearing capacity for ith realization;
$\bar{S}^a = \bar{S}^a_{\ln c_u}$;
$S_{\ln c_u}(\boldsymbol{x})$ = standard normal random field ($\ln c_u$);
$\bar{S}^a_{\ln c_u}$ = arithmetic average of $S_{\ln c_u}(\boldsymbol{x})$ over domain D;
s_c = shape factor;
v_c = coefficient of variation (COV);
w = active wedge zone depth in strip footing failure mechanism;
$\boldsymbol{x}, \boldsymbol{x}'$ = spatial points;
x, y, z = coordinate directions;
$\boldsymbol{x_i}$ = ith element location in space;
Φ = cumulative normal distribution function;
$\gamma(D) = \gamma(L_x, L_y, L_z)$ = variance reduction function over averaging domain D;
$\gamma(L_x)$, $\gamma(L_y)$ = variance functions used in calculating $\gamma(D)$;
$\gamma_x(L_y)$, $\gamma_y(L_x)$ = variance functions used in calculating $\gamma(D)$;
θ_{c_u} = scale of fluctuation of c_u;
θ^h = scale of fluctuation in horizontal direction;
$\theta^h_{\ln c_u}$ = scale of fluctuation of $\ln c_u$ in horizontal direction;
$\theta_{\ln c_u}$ = scale of fluctuation of $\ln c_u$;
θ^v = scale of fluctuation in vertical direction;
$\theta^v_{\ln c_u}$ = scale of fluctuation of $\ln c_u$ in vertical direction;
θ^y_x, θ^x_y = scale of fluctuation used in calculating $\gamma(D)$;
μ = mean;
μ_{M_c} = mean of M_c;
$\mu_{\ln M_c}$ = mean of $\ln M_c$;
μ_{c_u} = mean shear strength;
$\mu_{\ln c_u}$ = mean of $\ln c_u$;
$\mu_{\bar{c}_u}$ = mean of effective undrained shear strength;
μ_{q_f} = mean of ultimate bearing stress;
$\mu_{\ln q_f}$ = mean of logarithmic ultimate bearing stress;
ν = Poisson's ratio;
σ_{c_u} = standard deviation of c_u;
$\sigma_{\bar{c}_u}$ = standard deviation of effective undrained shear strength;
$\sigma_{\ln c_u}$ = standard deviation of $\ln c_u$;
$\sigma_{\ln M_c}$ = standard deviation of $\ln M_c$;
$\sigma_{\ln q_f}$ = standard deviation of logarithmic ultimate bearing stress;
σ_{M_c} = standard deviation of M_c;
σ_{q_f} = standard deviation of ultimate bearing stress;
σ = standard deviation;
$\boldsymbol{\tau} = \boldsymbol{x} - \boldsymbol{x}'$ = separation distance vector between two spatial points $\boldsymbol{x}$ and $\boldsymbol{x}'$;
τ_1, τ_2, τ_3 = separation distances in three coordinate directions; and
ϕ = friction angle in frictional soil.

References

Ahmed, A., and A.-H. Soubra. 2012. "Probabilistic analysis of strip footings resting on a spatially random soil using subset simulation approach." *Georisk: Assess. Manage. Risk Eng. Syst. Geohazards* 6 (3): 188–201. https://doi.org/10.1080/17499518.2012.678775.

Al-Bittar, T. 2012. "Probabilistic analysis of shallow foundations resting on spatially varying soils." Ph.D. thesis, Dept. of Civil Engineering, Univ. of Nantes.

Al-Bittar, T., and A.-H. Soubra. 2013. "Bearing capacity of strip footings on spatially random soils using sparse polynomial chaos expansion." *Int. J. Numer. Anal. Methods Geomech.* 37 (13): 2039–2060. https://doi.org/10.1002/nag.2120.

Al-Bittar, T., and A.-H. Soubra. 2014a. "Combined use of the sparse polynomial chaos expansion and the global sensitivity analysis for the probabilistic analysis of shallow foundations resting on a 3D random soil." In *Safety, reliability, risk and life-cycle performance of structures and infrastructures*, 3261–3268. New York: CRC Press.

Al-Bittar, T., and A.-H. Soubra. 2014b. "Efficient sparse polynomial chaos expansion methodology for the probabilistic analysis of computationally-expensive deterministic models." *Int. J. Numer. Anal. Methods Geomech.* 38 (12): 1211–1230. https://doi.org/10.1002/nag.2251.

Al-Bittar, T., A.-H. Soubra, and J. Thajeel. 2018. "Kriging-based reliability analysis of strip footings resting on spatially varying soils." *J. Geotech. Geoenviron. Eng.* 144 (10): 04018071. https://doi.org/10.1061/(ASCE)GT.1943-5606.0001958.

Bowles, J. 1996. *Foundation analysis and design*. New York: McGraw-Hill.

Ching, J., Y. Hu, and K. Phoon. 2015. "On the use of spatially averaged shear strength for the bearing capacity of a shallow foundation." In *Proc., 12th Int. Conf. on Applications of Statistics and Probability in Civil Engineering (ICASP12)*. Vancouver, BC, Canada: Univ. of British Columbia.

Ching, J., Y.-G. Hu, and K.-K. Phoon. 2016a. "On characterizing spatially variable soil shear strength using spatial average." *Probab. Eng. Mech.* 45 (Jul): 31–43. https://doi.org/10.1016/j.probengmech.2016.02.006.

Ching, J., S.-W. Lee, and K.-K. Phoon. 2016b. "Undrained strength for a 3D spatially variable clay column subjected to compression or shear." *Probab. Eng. Mech.* 45 (Jul): 127–139. https://doi.org/10.1016/j.probengmech.2016.03.002.

Ching, J., K.-K. Phoon, and P.-H. Kao. 2014. "Mean and variance of mobilized shear strength for spatially variable soils under uniform stress states." *J. Eng. Mech.* 140 (3): 487–501. https://doi.org/10.1061/(ASCE)EM.1943-7889.0000667.

Ching, J., K.-K. Phoon, and S.-P. Sung. 2017. "Worst case scale of fluctuation in basal heave analysis involving spatially variable clays." *Struct. Saf.* 68 (Sep): 28–42. https://doi.org/10.1016/j.strusafe.2017.05.008.

Chwała, M. 2019. "Undrained bearing capacity of spatially random soil for rectangular footings." *Soils Found.* 59 (5): 1508–1521. https://doi.org/10.1016/j.sandf.2019.07.005.

Der Kiureghian, A., and J.-B. Ke. 1987. "The stochastic finite element method in structural reliability." In *Stochastic structural mechanics*, 84–109. Berlin: Springer.

El Haj, A.-K., and A.-H. Soubra. 2020. "Efficient estimation of the failure probability of a monopile foundation using a Kriging-based approach with multi-point enrichment." *Comput. Geotech.* 121 (May): 103451. https://doi.org/10.1016/j.compgeo.2020.103451.

El Haj, A.-K., A.-H. Soubra, and J. Fajoui. 2019. "Probabilistic analysis of an offshore monopile foundation taking into account the soil spatial variability." *Comput. Geotech.* 106 (Feb): 205–216. https://doi.org/10.1016/j.compgeo.2018.10.011.

Fenton, G. A., and D. V. Griffiths. 1993. "Statistics of block conductivity through a simple bounded stochastic medium." *Water Resour. Res.* 29 (6): 1825–1830. https://doi.org/10.1029/93WR00412.

Fenton, G. A., and D. V. Griffiths. 2002. "Probabilistic foundation settlement on spatially random soil." *J. Geotech. Geoenviron. Eng.* 128 (5): 381–390. https://doi.org/10.1061/(ASCE)1090-0241(2002)128:5(381).

Fenton, G. A., and D. V. Griffiths. 2003. "Bearing-capacity prediction of spatially random c–φ soils." *Can. Geotech. J.* 40 (1): 54–65. https://doi.org/10.1139/t02-086.

Fenton, G. A., and D. V. Griffiths. 2004. "Reply to the discussion by R. Popescu on 'Bearing capacity prediction of spatially random c-φ soils'." *Can. Geotech. J.* 41 (2): 368–369. https://doi.org/10.1139/t03-080.

Fenton, G. A., and D. V. Griffiths. 2008. *Risk assessment in geotechnical engineering*. New York: Wiley.

Fenton, G. A., and E. H. Vanmarcke. 1990. "Simulation of random fields via local average subdivision." *J. Eng. Mech.* 116 (8): 1733–1749. https://doi.org/10.1061/(ASCE)0733-9399(1990)116:8(1733).

Griffiths, D., and G. A. Fenton. 2001. "Bearing capacity of spatially random soil: The undrained clay Prandtl problem revisited." *Géotechnique* 51 (4): 351–359. https://doi.org/10.1680/geot.2001.51.4.351.

Guo, X., and D. Dias. 2020. "Kriging based reliability and sensitivity analysis–Application to the stability of an earth dam." *Comput. Geotech.* 120 (Apr): 103411. https://doi.org/10.1016/j.compgeo.2019.103411.

Guo, X., D. Dias, C. Carvajal, L. Peyras, and P. Breul. 2019. "A comparative study of different reliability methods for high dimensional stochastic problems related to earth dam stability analyses." *Eng. Struct.* 188 (Jun): 591–602. https://doi.org/10.1016/j.engstruct.2019.03.056.

Hicks, M. A., and Y. Li. 2018. "Influence of length effect on embankment slope reliability in 3D." *Int. J. Numer. Anal. Methods Geomech.* 42 (7): 891–915. https://doi.org/10.1002/nag.2766.

Hicks, M. A., and K. Samy. 2002. "Influence of heterogeneity on undrained clay slope stability." *Q. J. Eng. Geol. Hydrogeol.* 35 (1): 41–49. https://doi.org/10.1144/qjegh.35.1.41.

Honjo, Y., and Y. Otake. 2013. "A simple method to assess the effects of soil spatial variability on the performance of a shallow foundation." In *Foundation engineering in the face of uncertainty: Honoring Fred H. Kulhawy*, 385–404. Reston, VA: ASCE.

Hu, Y.-G., and J. Ching. 2015a. "Impact of spatial variability in undrained shear strength on active lateral force in clay." *Struct. Saf.* 52 (Jan): 121–131. https://doi.org/10.1016/j.strusafe.2014.09.004.

Hu, Y.-G., and J. Ching. 2015b. "A new procedure for simulating active lateral force in spatially variable clay modeled by anisotropic random field." *J. Mech.* 31 (4): 381–390. https://doi.org/10.1017/jmech.2015.5.

Kawa, M., and W. Puła. 2019. "3D bearing capacity probabilistic analyses of footings on spatially variable c–φ soil." *Acta Geotech.* 2019 (Jul): 1–14. https://doi.org/10.1007/s11440-019-00853-3.

Kawa, M., W. Puła, and M. Suska. 2016. "Random analysis of bearing capacity of square footing using the LAS procedure." *Studia Geotechnica et Mechanica* 38 (3): 3–13. https://doi.org/10.1515/sgem-2016-0021.

Kuo, Y., M. Jaksa, A. Lyamin, and W. Kaggwa. 2009. "ANN-based model for predicting the bearing capacity of strip footing on multi-layered cohesive soil." *Comput. Geotech.* 36 (3): 503–516. https://doi.org/10.1016/j.compgeo.2008.07.002.

Lee, I. K., W. White, and O. G. Ingles. 1983. *Geotechnical engineering*. Melbourne, Australia: Pitman.

Li, D.-Q., X.-H. Qi, Z.-J. Cao, X.-S. Tang, W. Zhou, K.-K. Phoon, and C.-B. Zhou. 2015a. "Reliability analysis of strip footing considering spatially variable undrained shear strength that linearly increases with depth." *Soils Found.* 55 (4): 866–880. https://doi.org/10.1016/j.sandf.2015.06.017.

Li, J., Y. Tian, and M. J. Cassidy. 2014. "Failure mechanism and bearing capacity of footings buried at various depths in spatially random soil." *J. Geotech. Geoenviron. Eng.* 141 (2): 04014099. https://doi.org/10.1061/(ASCE)GT.1943-5606.0001219.

Li, J. H., Y. Zhou, L. L. Zhang, Y. Tian, M. J. Cassidy, and L. M. Zhang. 2016a. "Random finite element method for spudcan foundations in spatially variable soils." *Eng. Geol.* 205 (Apr): 146–155. https://doi.org/10.1016/j.enggeo.2015.12.019.

Li, L., J. Li, J. Huang, and F.-P. Gao. 2017a. "Bearing capacity of spudcan foundations in a spatially varying clayey seabed." *Ocean Eng.* 143 (Oct): 97–105. https://doi.org/10.1016/j.oceaneng.2017.05.026.

Li, L., J. Li, J. Huang, H. Liu, and M. J. Cassidy. 2017b. "The bearing capacity of spudcan foundations under combined loading in spatially variable soils." *Eng. Geol.* 227 (Sep): 139–148. https://doi.org/10.1016/j.enggeo.2017.03.022.

Li, Y. J. 2017. "Reliability of long heterogeneous slopes in 3D- model performance and conditional simulation." Ph.D. thesis, Dept. of Geoscience and Engineering, Delft Univ. of Technology.

Li, Y. J., M. A. Hicks, and J. D. Nuttall. 2015b. "Comparative analyses of slope reliability in 3D." *Eng. Geol.* 196 (Sep): 12–23. https://doi.org/10.1016/j.enggeo.2015.06.012.

Li, Y. J., M. A. Hicks, and P. J. Vardon. 2016b. "Uncertainty reduction and sampling efficiency in slope designs using 3D conditional random fields." *Comput. Geotech.* 79 (Oct): 159–172. https://doi.org/10.1016/j.compgeo.2016.05.027.

Li, Y. J., K. Liu, B. Zhang, and N. X. Xu. 2020. "Reliability of shape factors for bearing capacity of square footings on spatially varying cohesive soils." *Int. J. Geomech.* 20 (3): 04019195. https://doi.org/10.1061/(ASCE)GM.1943-5622.0001614.

Luo, N., and R. J. Bathurst. 2017. "Reliability bearing capacity analysis of footings on cohesive soil slopes using RFEM." *Comput. Geotech.* 89 (Sep): 203–212. https://doi.org/10.1016/j.compgeo.2017.04.013.

Matthies, H. G., C. E. Brenner, C. G. Bucher, and C. G. Soares. 1997. "Uncertainties in probabilistic numerical analysis of structures and solids-Stochastic finite elements." *Struct. Saf.* 19 (3): 283–336. https://doi.org/10.1016/S0167-4730(97)00013-1.

Meyerhof, G. G. 1951. "The ultimate bearing capacity of foundations." *Géotechnique* 2 (4): 301–332. https://doi.org/10.1680/geot.1951.2.4.301.

Nobahar, A. 2003. "Effects of soil spatial variability on soil-structure interaction." Ph.D. thesis, Faculty of Engineering and Applied Science, Memorial Univ. of Newfoundland.

Phoon, K.-K., and F. H. Kulhawy. 1999. "Characterization of geotechnical variability." *Can. Geotech. J.* 36 (4): 612–624. https://doi.org/10.1139/t99-038.

Popescu, R. 2004. "Discussion of 'Bearing capacity prediction of spatially random c-φ soils'." *Can. Geotech. J.* 41 (2): 366–367. https://doi.org/10.1139/t03-081.

Prandtl, L. 1920. "Über die härte plastischer körper." *Nachrichten von der Gesellschaft der Wissenschaften zu Göttingen, Mathematisch-Physikalische Klasse* 1920: 74–85.

Prandtl, L. 1921. "Hauptaufsätze: Über die eindringungsfestigkeit (härte) plastischer baustoffe und die festigkeit von schneiden." *J. Appl. Math. Mech.* 1 (1): 15–20. https://doi.org/10.1002/zamm.19210010102.

Puła, W., and M. Chwała. 2015. "On spatial averaging along random slip lines in the reliability computations of shallow strip foundations." *Comput. Geotech.* 68 (Jul): 128–136. https://doi.org/10.1016/j.compgeo.2015.04.001.

Puła, W., and M. Chwała. 2018. "Random bearing capacity evaluation of shallow foundations for asymmetrical failure mechanisms with spatial averaging and inclusion of soil self-weight." *Comput. Geotech.* 101 (Sep): 176–195. https://doi.org/10.1016/j.compgeo.2018.05.002.

Salgado, R., A. V. Lyamin, S. W. Sloan, and H. S. Yu. 2004. "Two-and three-dimensional bearing capacity of foundations in clay." *Géotechnique* 54 (5): 297–306. https://doi.org/10.1680/geot.2004.54.5.297.

Simoes, J. T., L. C. Neves, A. N. Antao, and N. M. Guerra. 2014. "Probabilistic analysis of bearing capacity of shallow foundations using three-dimensional limit analyses." *Int. J. Comput. Methods* 11 (2): 1342008. https://doi.org/10.1142/S0219876213420085.

Skempton, A. W. 1951. "The bearing capacity of clays." In *Proc., Building Research Congress*, 180–189. London: Thomas Telford. https://doi.org/10.1680/sposm.02050.0008.

Smith, I. M., and D. V. Griffiths. 2005. *Programming the finite element method*. New York: Wiley.

Soubra, A.-H., T. Al-Bittar, J. Thajeel, and A. Ahmed. 2019. "Probabilistic analysis of strip footings resting on spatially varying soils using kriging metamodeling and importance sampling." *Comput. Geotech.* 114 (Oct): 103107. https://doi.org/10.1016/j.compgeo.2019.103107.

Stuedlein, A. W., S. L. Kramer, P. Arduino, and R. D. Holtz. 2012. "Reliability of spread footing performance in desiccated clay." *J. Geotech. Geoenviron. Eng.* 138 (11): 1314–1325. https://doi.org/10.1061/(ASCE)GT.1943-5606.0000706.

Terzaghi, K. 1943. *Theoretical soil mechanics*. New York: Wiley.

Vahdatirad, M. J., L. V. Andersen, L. B. Ibsen, J. Clausen, and J. D. Sørensen. 2013. "Probabilistic three-dimensional model of an offshore monopile foundation: Reliability based approach." In *Proc., 7th Int. Conf. on Case Histories in Geotechnical Engineering*. Chicago: Missouri Univ. of Science and Technology.

van den Eijnden, A., and M. Hicks. 2017. "Efficient subset simulation for evaluating the modes of improbable slope failure." *Comput. Geotech.* 88 (Aug): 267–280. https://doi.org/10.1016/j.compgeo.2017.03.010.

Vanmarcke, E. H. 1977. "Probabilistic modeling of soil profiles." *J. Geotech. Eng. Div.* 103 (11): 1227–1246. https://doi.org/10.1061/AJGEB6.0000517.

Vanmarcke, E. H. 1978. "Probabilistic characterization of soil profiles." In *Site characterization & exploration*, 199–219. Reston, VA: ASCE.

Vanmarcke, E. H. 1983. *Random fields: Analysis and synthesis*. Cambridge, MA: MIT Press.

Vanmarcke, E. H., and M. Grigoriu. 1983. "Stochastic finite element analysis of simple beams." *J. Eng. Mech.* 109 (5): 1203–1214. https://doi.org/10.1061/(ASCE)0733-9399(1983)109:5(1203).

Zhou, S., X. Guo, Q. Zhang, D. Dias, and Q. Pan. 2020. "Influence of a weak layer on the tunnel face stability—Reliability and sensitivity analysis." *Comput. Geotech.* 122 (Jun): 103507. https://doi.org/10.1016/j.compgeo.2020.103507.